Nat. Hazards Earth Syst. Sci. Discuss., doi:10.5194/nhess-2016-60, 2016
Manuscript under review for journal Nat. Hazards Earth Syst. Sci.
Published: 25 February 2016
© Author(s) 2016. CC-BY 3.0 License.

Natural Hazards and Earth System Sciences
Discussions

Comparison and validation of global and regional ocean forecasting systems in the South China Sea

Xueming Zhu[1], Hui Wang[1], Guimei Liu[1*], Charly Régnier[2], Xiaodi Kuang[1], Dakui Wang[1], Shihe Ren[1], Zhiyou Jing[3], Marie Drévillon[2]

[1]Key Laboratory of Research on Marine Hazards Forecasting, National Marine Environmental Forecasting Center, Beijing, 100081, China
[2]Mercator Océan, Ramonville Saint Agne, France
[3]State Key Laboratory of Tropical Oceanography, South China Sea Institute of Oceanology, Chinese Academy of Sciences, Guangzhou, 510301, China

Correspondence to: Guimei Liu (liugm@nmefc.gov.cn)

Abstract. In this paper, the performances of two operational ocean forecasting systems, Mercator Océan (MO) in France and South China Sea Operational Forecasting System (SCSOFS) in China, have been examined. Both systems can provide science-based nowcast/forecast products, such as temperature, salinity, water level and ocean circulations. Based on the observed satellite and *in-situ* data have been obtained in 2012 in the South China Sea, the comparison and validation of the ocean circulations, the structures of the temperature and salinity, and some mesoscale activities are shown. Comparing with the observation, the ocean circulations and SST of MO show better results than those of SCSOFS. However, the structures of temperature and salinity of SCSOFS are better than those of MO. For the mesoscale activities, SST fronts and SST decreasing during the typhoon Tembin of SCSOFS are better agreement with the previous study or satellite data than those of MO; but both of them show some differences from AVISO data. Finally, according to the results compared in above, some suggestions have been proposed for both systems to improve their performances in the near further.

Keywords. SCSOFS, Mercator Océan, South China Sea, Operational Forecasting System

1 Introduction

The South China Sea (SCS, Fig.1) is the largest and deepest semi-enclosed marginal sea of the Northwestern Pacific (NWP), with the area is about 3.5 million km^2, the mean and maximum depth is about 1200m and 5300m, respectively. A wide continental shelf with depth less than 200m located in the northern SCS (NSCS). There are numerous islands, reefs, beaches, shoals in large basin of the southern

Nat. Hazards Earth Syst. Sci. Discuss., doi:10.5194/nhess-2016-60, 2016
Manuscript under review for journal Nat. Hazards Earth Syst. Sci.
Published: 25 February 2016
© Author(s) 2016. CC-BY 3.0 License.

Natural Hazards and Earth System Sciences
Discussions

SCS (SSCS). It is connected with the adjacent seas through a number of channels, to the East China Sea in north, the NWP in east, the Sulu Sea in southeast, and the Java Sea in south, by the Taiwan Strait (TWS), the Luzon Strait (LUS), the Mindoro Strait and the Balabac Strait, the Karimata Strait, respectively. Its unique geographical features, rich marine mineral and petroleum resources play a significant role to many countries adjacent to it.

The SCS is located in the East Asian Monsoon (EAM) winds regime, the northeastly winds usually prevail with an average wind speed of 9m/s over the whole domain in winter, while the southwestly winds prevail with an average magnitude of 6m/s dominating over the most parts of the SCS in summer (Hellerman and Rosenstein, 1983). The EAM is considered to be the main factor for driving the upper layer basin-scale circulation pattern in the entire SCS, showing an obvious seasonal variation with a cyclonic gyre in winter and an anti-cyclonic gyre in summer (Wyrtki, 1961; Mao et al., 1999; Wu et al., 1999; Qu, 2000; Chu and Li, 2000). However, some other literatures insist that a persistent cyclonic gyre in the NSCS, while a biannually changing from cyclonic gyre in winter to anti-cyclonic gyre in summer in the SSCS (Chao et al., 1996; Takano et al., 1998; Hu et al., 2000; Chern and Wang, 2003; Caruso et al., 2006; Chern et al., 2010). Chern et al. (2010) suggested that the three dynamical processes, the wind stress curl, the deep-water ventilation-induced vortex stretching in the central SCS, and a positive vorticity generated from the left flank of the Kuroshio in the LUS, play the equal importance to the formation of the persistent cyclonic gyre in the NSCS, according to the analysis of the results from several numerical experiments with different wind stress, topography and coastline.

In addition to the basin-scale circulations, there are still some sub-basin scale currents in the SCS, such as the Guangdong coastal current (Huang et al., 1992), the SCS Warm Current (SCSWC, Guan, 1978; Chao et al., 1995), Dongsha Coastal Current (DCC, Su, 2005), Luzon Coastal Current (LCC, Hu et al., 2000), and so on. However, there are still a lot of debates about the mechanisms of some of them among the studies reported by several authors, without reaching an agreement. For example, based on the results of the numerical simulations, the formation dynamical mechanism of the SCSWC may be related to the Kuroshio intrusion (Li et al., 1993; Cai and Wang, 1997), sea surface slope (Fang and Zhao, 1988; Guan, 1993), or the wind relaxation (Chao et al., 1995).

The Kuroshio intrudes into the SCS through the LUS, carrying the warm and salty water from the NWP, significantly affecting the circulation pattern and the budgets of heat and salt in the NSCS (Farris and Wimbush, 1996; Wu and Chiang, 2007; Liang et al., 2008; Nan et al., 2013). However, it is still not in

Nat. Hazards Earth Syst. Sci. Discuss., doi:10.5194/nhess-2016-60, 2016
Manuscript under review for journal Nat. Hazards Earth Syst. Sci.
Published: 25 February 2016
© Author(s) 2016. CC-BY 3.0 License.

accordance with how the Kuroshio intrudes into the NSCS. As pointed out in Hu et al. (2000), there existed four viewpoints on the Kuroshio intrusion as, a direct branch from the Kuroshio (Williamson, 1970; Fang et al., 1996; Chern and Wang, 1998; Qu et al., 2000), a form of loop (Zhang et al., 1995; Liu et al., 1996; Farris and Wimbush, 1996), a form of extension (Hu et al., 1999), and a form of ring (Li et al., 1998a, b) at present. Nan et al. (2015) reviewed and summarized the Kuroshio intruding processes from observed data, numerical experiments and theoretical analyses, and concluded that there were three typical paths of the Kuroshio intruding the SCS, the looping path, the leaking path and the leaping path, which could be distinguished quantitatively by a Kuroshio SCS Index (KSI, Nan et al., 2011a) derived from the integral of geostrophic vorticity southwest of Taiwan. The three paths can change from one to another in several weeks.

In addition, many mesoscale eddy activities are another obvious physical characteristics of the NSCS, and play a great influence on the dynamical environment of the NSCS. Eddies are generally more energetic than the surrounding currents and are an important component of dynamical oceanography at all scales. In particular they transport heat, mass, momentum and biogeochemical properties from their regions of formation to remote areas where they can then impact budgets of the tracers. Eddies in the NSCS have attracted increasing attention over recent a few decades. Much work has been done based on the combination of satellite observation and *in-situ* hydrographic data (Wang and Chern, 1987; Li et al., 1998; Chu et al., 1999; Wang et al., 2003; Hu et al., 2011; Nan et al., 2011b), or numerical models (Wu and Chiang, 2007; Xiu et al., 2010; Zhuang et al., 2010). Some of work has been focused on the statistical characteristics of eddies in the SCS, but they are greatly different from each other, owing to different criteria for eddy identification employed by different literatures (Wang et al., 2003; Xiu et al., 2010; Du et al., 2014). Some of work analyzes eddies' seasonal variability (Wu and Chiang, 2007; Zhuang et al., 2010) and investigates their genesis (Wang et al., 2008). Some of work mainly studies specific eddies to better understand eddy's generation, development and disappearance mechanisms (Wang et al., 2008; Zhang et al., 2013).

As shown above, the dynamic processes and relative mechanisms are very complex, but still not cleared until now in the SCS. It will be much more difficult to predict the status of the future ocean. National Marine Environmental Forecasting Center (NMEFC) is mainly responsible for the prediction of the sea area of the South China Sea, has built a SCS Operational Forecasting System (SCSOFS). As is known to all, the open boundary forcing plays an important role in the numerical prediction of the regional ocean.

Nat. Hazards Earth Syst. Sci. Discuss., doi:10.5194/nhess-2016-60, 2016
Manuscript under review for journal Nat. Hazards Earth Syst. Sci.
Published: 25 February 2016
© Author(s) 2016. CC-BY 3.0 License.

Natural Hazards and Earth System Sciences Discussions

Due to the various limitations, the current SCSOFS' open boundary conditions (OBC) are derived from the Simple Ocean Data Assimilation (SODA) climatological monthly mean during the forecast run. It is extremely inappropriate for the real-time ocean prediction system, so we plan to transform the OBC from SODA to the real-time forecasting results derived from Mercator Océan (MO) on the next step, in order to further improve prediction accuracy of the SCSOFS. Before carrying out this work, it is necessary to compare and validate the performance of MO in the SCS.

The focusing of this paper will be the comparison and validation of the performances of MO and SCSOFS in the SCS, based on the observation data we have got in 2012. The rest of this paper is organized as follows. Section 2 gives the introductions to the observed data which are employed to validate the systems, and the configurations of MO and SCSOFS. Section 3 shows the results of comparison and validation and discussions. Section 4 presents the summary and conclusions.

2 Observed data and numerical operational systems

2.1 Satellite data

The Map of Sea Level Anomaly (MSLA) and Map of Absolute Dynamic Topography (MADT) data, also with the relative Geostrophic Velocity Anomaly (GVA) and Absolute Geostrophic Velocity (AGV) data derived from them, respectively, are used to analysis the mesoscale eddy in the SCS and compare with the numerical simulations. They are all-sat-merged and gridded delayed-time altimeter product produced by SSALTO/DUACS and distributed by Aviso in April 2014, with support from Centre National D'études Spatiales (Cnes, www.aviso.altimetry.fr). The products are sampled on a 0.25 °×0.25 ° resolution Cartesian grid in both longitude and latitude from the Mercator gridded product, with a daily temporal resolution. Its period covers from 1993 to present, and the period of reference has been changed from 7 years (1993-1999) to 20 years (1993-2012). It has been corrected for instrumental errors, environmental perturbations, the ocean sea state influence, the tide influence, atmospheric pressure and multi-mission cross-calibration (CLS, 2015).

Two kinds of Sea Surface Temperature (SST) data will be used in this paper. One is derived from the merged satellite (NOAA/AVHRR, MetOp/AVHRR, GCOMW1/AMSR2, Coriolis/WINDSAT) and *in-situ* data Global Daily SST (MGDSST), with a 0.25 °×0.25 ° horizontal resolution, which is analyzed

Nat. Hazards Earth Syst. Sci. Discuss., doi:10.5194/nhess-2016-60, 2016
Manuscript under review for journal Nat. Hazards Earth Syst. Sci.
Published: 25 February 2016
© Author(s) 2016. CC-BY 3.0 License.

and published by Japan Meteorological Agency (JMA). The data can be obtained from http://near-goos1.jodc.go.jp/.

The other one is derived from the NOAA 1/4 ° daily Optimum Interpolation Sea Surface Temperature (OISST), which is an analysis constructed by combining observations from different platforms, such as satellites, ships, buoys, on a regular grid via optimum interpolation. Right now, National Centers for Environmental Information (NCEI) provides two kinds of OISST: one uses infrared satellite data from the Advanced Very High Resolution Radiometer (AVHRR) named as AVHRR-only, and the other one uses AVHRR data along with microwave data from the Advanced Microwave Scanning Radiometer (AMSR) on the Earth Observing System Aqua or AMSR-E satellite named as AVHRR+AMSR. The first one, AVHRR-only, is used in this study, which spans 1981 to the present and can be downloaded from the website http://www.ncdc.noaa.gov/oisst/data-access.

2.2 *In-situ* data

The *in-situ* data employed in this paper for the comparison and validation of both systems are provided by the South China Sea Institute of Oceanology, Chinese Academy of Sciences. There were one mooring to measure the sea water velocity and 5 cruises implemented to measure the temperature and salinity (TS) in the SCS during 2012.

The mooring station is located at Maoming (Fig. 1), where bottom-mounted upward-looking 75 kHz Acoustic Doppler Current Profilers (ADCPs) are deployed to monitor the current profile (U component and V component) from the depth of 2m to 48m with a 2-m interval in vertical. The period of the monitoring is from 11 July to 8 October, in 2012, with a temporal interval 10 min. Firstly, the abnormal data are eliminated from the original measured data; in the second, a low-pass filter with 25-hour is applied to filter out the tidal current; and a 25-hour average is calculated to get the daily average data, in order to compare and validate with the simulated results of MO and SCSOFS.

The TS data from 5 cruises are measured by SeaBird 19 plus conductivity-temperature-depth (CTD) with 1-m resolution in vertical. Among the 5 cruises, one is the Qiongdong cruise in the NSCS, which was conducted 9 days from 12 to 20 July at 90 stations along 6 sections (See Fig.1); another one is the Nansha cruise around the Nansha Islands, which was conducted 5 days from 24 to 28 August at 17 stations along 10 °N section from 109.5 °E to 117.5 °E. The TS data from those two cruises will be used to compare and validate the TS distribution from MO and SCSOFS in vertical and horizontal. All the measured TS data

Nat. Hazards Earth Syst. Sci. Discuss., doi:10.5194/nhess-2016-60, 2016
Manuscript under review for journal Nat. Hazards Earth Syst. Sci.
Published: 25 February 2016
© Author(s) 2016. CC-BY 3.0 License.

from 5 cruises will be collected to compare with the simulated data from MO and SCSOFS via correlation analysis.

2.3 The configurations of SCSOFS

The SCSOFS is build up based on the Regional Ocean Modelling System (ROMS), which is a three-dimensional, non-linear primitive equations, free surface, hydrostatic, split-explicit, topography-following-coordinate in vertical and orthogonal curvilinear in horizontal on a staggered Arakawa C-grid oceanic model (Shchepetkin and McWilliams, 2005).

To avoid the influences of boundary to the circulations in the SCS, the model's boundaries was extended to southward and eastward, then the model covered a larger domain (4.5 °S to 28.3 °N, 99 °E to 145 °E, Fig. 1) than the SCS. The horizontal resolution variates from 1/12 °in the south and east boundary to 1/30 °in the SCS. There were 36 s-coordinate levels in the vertical with the thinnest layer being 0.16 m on the surface. The bathymetry was extracted from the ETOPO1 data sets published by U.S. National Geophysical Data Center (NGDC), which is a global relief model of Earth's surface that integrates ocean bathymetry and land topography, with 1 arc-minute resolution (Amante and Eakins, 2009). The ETOPO1 data has combined the satellite altimeter observations, shipping load sonar measurement, multi resolutions digital terrain database and the global digital terrain model and many other sources, and been used in the global and regional oceanic model widely. And the original bathymetry was revised in the area of next to the coast of China mainland according to the *in-situ* data measured by our group, then smoothed according to Shapiro (1975). The maximum depth was set to be 6000 m and the minimum depth to be 10 m in the model (Wang, 1996).

The initial temperature and salinity were derived from the climatology monthly mean Simple Ocean Data Assimilation (SODA, Carton and Giese, 2008) in January. However, the initial velocities and elevation were set to zero, which means to integrate the model from a static status. The model's western lateral boundary was treated as a wall. The other three (northern, southern, eastern) lateral boundaries were opened, whose temperature, salinity, velocity, and elevation were prescribed by spatial interpolation of the monthly mean SODA dataset. The 2D and 3D velocities, through the open boundaries, are modulated to guarantee the conservation of volume flux in the whole model domain. In addition, the nudging technology was used for 3D velocity, temperature, and salinity to the three open lateral boundaries with a 30-day time scale for outflow and 3-day for inflow.

Nat. Hazards Earth Syst. Sci. Discuss., doi:10.5194/nhess-2016-60, 2016
Manuscript under review for journal Nat. Hazards Earth Syst. Sci.
Published: 25 February 2016
© Author(s) 2016. CC-BY 3.0 License.

The model is forced using 6-hourly wind stress, net fresh water flux, net heat flux, surface solar shortwave radiation at surface from NCEP_Reanalysis 2 data provided by the NOAA/OAR/ESRL PSD, Boulder, Colorado, USA, from their web site at http://www.esrl.noaa.gov/psd/ (Kanamitsu et al., 2002). In order to get more reasonable simulated SST, the kinematic surface net heat flux sensitivity to SST (dQ/dSST) is used to introduce thermal feedback to correct net surface heat flux (Barnier et al., 1995) with a constant number -30 $W/m^2/℃$ in the whole domain. In addition, the monthly mean climatology discharges of the Mekong River and the Pearl River are prescribed to the model.

The system was run with 6 seconds time step for the external mode, and 180 seconds for the internal mode under the initial conditions, boundary conditions and surface forcing mentioned in above. The system was conducted a hindcast run from 2000 to 2011 after a 15 years climatology run for spin-up (Wang et al., 2012). The model results are archived to the snapshot with a 5-day interval, which will be used as the ensemble members for the EnOI (Ensemble Optimal Interpolation) method assimilation. After the hindcast run, the system was conducted an assimilation run in 2012 with EnOI method, the along track SLA data from AVISO had been assimilated as the observations with a 7-day time window. The details on the EnOI applied in the SCSOFS can be referred as Ji et al. (2015). The assimilated results are archived to daily mean with a 1-day interval in 2012, which will be used to compare and validate in this paper. Then the system is operating in NMEFC since January 1st, 2013. It runs daily for 6 days (1-day nowcast and 5-day forecast), and provides 120-hour forecasting products, which including the 3D ocean temperature, salinity and currents with 24 hours interval.

2.4 The configurations of MO

The high resolution global analysis and forecasting system PSY4V1R3 was operational as the V2 of the MyOcean project from February 2011 up to April 2013, when it was replaced by the PSY4V2R2 system. During this period, PSY4V1R3 has been producing weekly 14-day hindcasts and daily 7-day forecasts. The model configuration of PSY4V1R3 is based on a tripolar ORCA grid type (Madec and Imbard, 1996) in the NEMO 1.09 version with a 1/12 °horizontal resolution which means 9 km at the Equator, 7 km at mid latitudes and 2km toward the Ross and Weddel Sea. The grid cells follow an Arakawa C-grid type (Arakawa and Lamb, 1977). The 50-level vertical discretization retained in this system has 1m resolution at the surface, decreasing to 450m at the bottom and 22 levels within the upper 100m. “Partial cell” parametrization was chosen for a better representation of the topographic floor (Barnier et al., 2006). The

Nat. Hazards Earth Syst. Sci. Discuss., doi:10.5194/nhess-2016-60, 2016
Manuscript under review for journal Nat. Hazards Earth Syst. Sci.
Published: 25 February 2016
© Author(s) 2016. CC-BY 3.0 License.

Natural Hazards and Earth System Sciences
Discussions

high frequency gravity waves are filtered out by the free surface formulation of Roullet and Madec (2000).

For the diffusion, a horizontal bilaplacian was added along the equator ($20 m^2 s^{-1}$) and two laplacians in the Canadian straits (up to $100 m^2 s^{-1}$). Laplacian lateral isopycnal diffusion was added on tracers (125 $m^2 s^{-1}$) and a horizontal biharmonic viscosity was added for the momentum (-1×1010 $m^4 s^{-1}$ at the Equator and decreasing poleward as the cube of the grid size). In addition, the vertical mixing is parameterized according to a turbulent closure model (TKE order 1.5) adapted by Blanke and Delecluse (1993), the lateral friction condition is a partial-slip condition with a regionalization for the Mediterranean Sea, Indonesian region, Canadian straits and Cape Horn. The atmospheric fields are taken from the ECMWF (European Centre for Medium Range Weather Forecasts) Integrated Forecast System at a daily average frequency. Momentum and heat turbulent surface fluxes are computed from CLIO bulk formulae (Goosse et al., 2001). We use a viscous-plastic rheology formulation for the LIM2_VP ice model (Fichefet and Maqueda, 1997, LIM2_VP in Hunke and Dukowicz 1997,). A multivariate data assimilation (Kalman Filter kernel with SEEK formulation , Pham et al., 1998) of *in-situ* T and S (from Coriolis/Ifremer), along track MSLA (from AVISO, with MDT from Rio and Hernandez, 2004) and intermediate resolution SST (1/4 °SST product RTG from NOAA) is performed with the SAM2 software (Lellouche et al., 2013). An Incremental Analysis Update (IAU) centered on the 4th day of the 7-day assimilation window ensures a smooth correction of T, S, U, V and SSH. The assimilation cycle consists of a first 7-day simulation called guess or forecast, at the end of which the analysis takes place. The IAU correction is then computed and the model is re-run on the same week, progressively adding the correction. The increment is distributed in time with a Gaussian shape which is centered on the 4th day. More details on the SAM2 software (applied on other model configurations) can be found in Lellouche et al. (2013) except that no large scale bias correction is applied in PSY4V1R3. Concerning the initial conditions, the PSY4V1R3 was started in April 2009 from a 3D climatology of temperature and salinity (WOA2005).

Nat. Hazards Earth Syst. Sci. Discuss., doi:10.5194/nhess-2016-60, 2016
Manuscript under review for journal Nat. Hazards Earth Syst. Sci.
Published: 25 February 2016
© Author(s) 2016. CC-BY 3.0 License.

Natural Hazards and Earth System Sciences Discussions

3 Comparisons, validations and discussion

3.1 Velocities

3.1.1 Absolute Geostrophic Velocity

Figure 2 shows the distributions of the monthly AGV composited with Sea Surface Height (SSH) from AVISO, MO, and SCSOFS in January, April, July, and October of 2012, respectively. Here we use the January, April, July, and October represent winter, spring, summer, and autumn, respectively. It is valuable to note that the AGV of MO and SCSOFS are not the velocities output from the numerical model directive. However, in order to better comparison, they are recalculated according to SSH from the model output on every day and assuming geostrophic balance following Eq. (1):

$$u = -\frac{g}{f}\frac{\partial SSH}{\partial y} \qquad v = \frac{g}{f}\frac{\partial SSH}{\partial x} \tag{1}$$

where g is gravitation acceleration, f is the Coriolis parameter, x, y are the east, north axis; u, v are the eastward, northward velocity components in horizontal, respectively.

By comparing among the three results, both MO and SCSOFS can catch the main basin-scale oceanic circulation pattern in the SCS, and show that a cyclonic gyre in winter and an anti-cyclonic gyre in summer, which being well accordance with the pattern of AVISO, except that the current speeds are a little stronger than AVISO. It is worth to mention that the result of MO is well agreement with the AVSIO in January, such as the southward western boundary currents along the eastern coast of Vietnam, the LCC, the anti-cyclonic eddy in the western of the LUS around (118 °E, 21 °N), the cyclonic eddy in the eastern of the Vietnam around (113 °E, 15 °N). However, the result of SCSOFS is much smooth without obvious mesoscale or small scale circulation, or they are very weaker (0.2-0.4m s^{-1}) than those (0.6-0.8m s^{-1}) of AVISO or MO. The circulation is chaos in spring in the SCS, though the circulation pattern of MO is better agreement with the one of AVISO than the one of SCSOFS. All the three results show the anti-cyclonic eddy around (111 °E, 10 °N) and the western boundary jet in the southeast of the Vietnam in summer, with the maximum speed being about 1.0m s^{-1}, 0.9m s^{-1}, and 0.7m s^{-1} for AVISO, MO, SCSOFS, respectively. The westward intensification along the eastern coast of the Vietnam is most obvious in autumn than other three seasons, and the maximum speed is more than 1.0m s^{-1} for MO and SCSOFS, but 0.7m s^{-1} for AVISO.

As mentioned in Sect. 1, the Kuroshio intruding the SCS through the LUS has been distinguished three types as the looping path, the leaking path and the leaping path, according to Nan et al. (2011a). All three

Nat. Hazards Earth Syst. Sci. Discuss., doi:10.5194/nhess-2016-60, 2016
Manuscript under review for journal Nat. Hazards Earth Syst. Sci.
Published: 25 February 2016
© Author(s) 2016. CC-BY 3.0 License.

results show the looping path in winter, the leaping path in summer and leaking path in autumn, which is well accordance with the model results showed by Wu and Chiang (2007). However, AVISO, MO, and SCSOFS show the leaking path, looping path, and leaping path in spring, respectively.

3.1.2 Time series from mooring station

Figure 3 shows the comparison of the daily mean time series of the u, v components from the mooring, MO, and SCSOFS in 40m-depth layer at the Maoming station (See Fig. 1) from July 11 to October 8, 2012. Both MO and SCSOFS can catch the same variation trends of the time series with the mooring observation. Especially, MO results have represented the current variations well for both u- and v-component, during the period of the Typhoon Kai-tak on 17 August 2012. Although SCSOFS shows the larger velocity during the Typhoon Kai-tak, the range of large is less than the observation and leading the observation about 1 day. The root mean square errors (RMSE) between MO and SCSOFS and observation are 0.075m s^{-1}, 0.094m s^{-1} for u-component, 0.062m s^{-1}, 0.084m s^{-1} for v-component, respectively. Overall, MO results are better agreement with the observation than those of SCSOFS. However, SCSOFS results have a phase bias comparing with the observation, which is leading the observation about 1 day.

3.2 Temperature and Salinity

3.2.1 SST

SST is a very important prognostic variable in a hydrostatic ocean general circulation numerical model, which plays a key role to the ocean circulations and the air-sea interaction. So SST error is crucial criteria of the numerical model skill, especially for an operational ocean circulation model. In fact, the SST simulation error is affected by several factors, for example the limitation of physical model, the surface atmosphere forcing, the bias of initial field and the uncertainty from the open boundary, as pointed out by Ji et al. (2015). Although the SST data have been assimilated into both MO and SCSOFS, the assimilated SST still has some errors for both systems.

Figure 4 shows the distributions of the monthly mean SST errors between two systems and MGDSST in the SCS in 2012. The errors show an obvious regional distribution, the bigger errors mainly exist in the coastal region for the depth shallower than 200 m, such as in the TWS, the eastern of the Guangdong province in January, the gulf of Tonkin in July. What's more, the strong seasonal variation for SST error

Nat. Hazards Earth Syst. Sci. Discuss., doi:10.5194/nhess-2016-60, 2016
Manuscript under review for journal Nat. Hazards Earth Syst. Sci.
Published: 25 February 2016
© Author(s) 2016. CC-BY 3.0 License.

also can be found, which is larger in winter and smaller in summer, from both systems. Comparing with MGDSST, the maximum, minimum, and mean monthly RMSE are 0.78℃, 0.37℃, 0.51℃ for the MO, 1.15℃, 0.56℃, 0.86℃ for the SCSOFS, respectively, in the SCS. Based on the Fig. 4, the simulated SST performance of MO is better than those of SCSOFS by comparing with MGDSST.

3.2.2 Horizontal and vertical distribution of TS

The horizontal distributions of 10-m depth layer TS in the eastern of Hainan island from the *in-situ* of Qiongdong cruise, MO, and SCSOFS, respectively, are shown in Fig. 5. Two clear cold and salty water cores located at the eastern of Hainan island, which being about (110.75 °E, 19.2 °N) and (111.3 °E, 19.7 °N), are shown in both *in-situ* and SCSOFS (Fig. 5), except that the SCSOFS being more saline than *in-situ*. It can be easily deduced that the two cores are produced by upwelling process from the TS vertical distributions of the section K, F, H, and G (Jing et al., 2015).

Figure 6 shows the vertical TS distributions from the *in-situ* of Qiongdong cruise, MO and SCSOFS, along section E. Both systems have got the same vertical structures of TS with the *in-situ*. All of them show out the obvious upwelling system, with cold and salty waters flowing from offshore to nearshore along the bottom. All three results show the upper mixing layer depth is about 15m, with the sea water well mixed above 15m depth and the isotherms and isohalines are almost vertical, indicating strong stratification in summer. The diluted water is flushing from the nearshore to offshore, with the 33-isohaline located at about 50km for both *in-situ* and SCSOFS, but at about 20km for MO. In above, it is indicated that the results of SCSOFS is better agreement with the *in-situ* than those of MO.

The vertical distributions of TS from the *in-situ* of Nansha cruise, MO, and SCSOFS along the 10 °N section are shown in Fig.7 for the layer above 300m and Fig.8 for the layer of 300-1200m. Both systems have got almost the same vertical structures with the *in-situ*, especially for the upper mixing layer depth about 70m are shown in the three results. The temperature almost linearly decreases from 28℃ to 3℃ with the depth increasing from the bottom of the upper mixing layer to the 1200m depth. However, the salinity increases from 33.5 to 34.5 with the depth increasing from the bottom of the upper mixing layer to about 200m depth, and keeps 34.5 from 200m to 300m depth. Then a fresh water layer exists in the middle layer from about 400m to 700m with the salinity about 34.4. Below the middle layer, the salinity again increases from 34.4 to 34.58 with the depth increasing from 700m to 1200m. It indicates that the results of MO and SCSOFS are well agreement with *in-situ*, except that the salinity of the fresh water in

Nat. Hazards Earth Syst. Sci. Discuss., doi:10.5194/nhess-2016-60, 2016
Manuscript under review for journal Nat. Hazards Earth Syst. Sci.
Published: 25 February 2016
© Author(s) 2016. CC-BY 3.0 License.

the middle layer from MO is less than 34.4 and fresher than those of *in-situ* and SCSOFS, but the thickness of the layer is thicker than those of *in-situ* and SCSOFS.

3.2.3 Correlation ship between model and *in-situ*

In order to better compare and validate the performances of the two systems, we collected all the measured TS data from five cruises in the SCS in 2012 to conduct a comprehensive correlation analysis. Figure 9 shows the comparison of relativity of TS between MO, SCSOFS and *in-situ* by scatter points, respectively. Any point in the Fig.9 is corresponded with two values of temperature or salinity, one is from the *in-situ* along X axis, and the other one is from MO or SCSOFS along Y axis. The correlation coefficients of temperature are 0.987, 0.982, and of salinity are 0.717, 0.897, between MO, SCSOFS and *in-situ*, over the 95% significance level, respectively, which showing the good relativity between MO, SCSOFS and *in-situ*. It also indicates that the relativity of temperature is better agreement with *in-situ* than those of salinity for both MO and SCSOFS, and SCSOFS is better agreement with *in-situ* than MO for salinity.

3.3 Mesoscale activities

3.3.1 SST front

Oceanic front is a good indicator for connection between water masses with different hydrological features, which is an important marine mesoscale phenomenon. There are numerous SST fronts in the SCS, most of them located on the continental shelf with the depth below 200m or aligned with the shelf break, especially in the NSCS. A few evident SST fronts have been identified from the long-term NOAA/NASA Pathfinder SST data, namely: Fujian-Guangdong Coastal Front, Pear River Estuary Coastal Front, Taiwan Bank Front, Kuroshio Intrusion Front, Hainan Island East Coastal Front, Tonkin Gulf Coastal Front (Wang et al., 2001). All of them exhibit very strong seasonal variability, which is mainly due to the EAM (Belkin and Cornillon, 2003).

Figure 10 shows the distributions of SST fronts from MO and SCSOFS for four seasons. The similar frontal patterns with their evident seasonal variations are shown in both systems, except for some small differences. In winter, most fronts reach maximum strength (>0.2℃/km). The Fujian-Guangdong coastal front and Taiwan Bank front are major fronts in the SCS which agree with previous satellite result from Wang et al. (2001). These two fronts merge and extend to Pearl River Estuary and the Hainan Island. The

Nat. Hazards Earth Syst. Sci. Discuss., doi:10.5194/nhess-2016-60, 2016
Manuscript under review for journal Nat. Hazards Earth Syst. Sci.
Published: 25 February 2016
© Author(s) 2016. CC-BY 3.0 License.

Hainan Island East Coastal Front is stronger in MO than in SCSOFS, whereas the Tonkin Gulf Coastal Front is stronger in SCSOFS than in MO. In SCSOFS, the Kuroshio Intrusion front is obvious, however, which is hardly seen in MO. In spring, most fronts become weak obviously due to the weakening of northeast monsoon from both systems, except that the Hainan West Coastal front emerges in SCSOFS. In summer, weakening almost occurs in all the fronts mentioned above for SCSOFS, which is in agreement with the result of Wang et al. (2001). However, disappearing occurs in all the fronts for MO. In fall, most fronts fade and disappear, except that the Taiwan Bank front has very weak strength compared to other seasons for both systems. Both systems have not shown the Kuroshio Intrusion Front identified by Wang et al. (2001) in summer and fall.

3.3.2 The Typhoon Tembin

There are a lot of typhoons in the SCS during the typhoon season in every year, so that the typhoon activities are very frequent in the SCS, especially in 2012. One hot study on the air-sea interaction is the responding of the physical ocean dynamics to typhoon in the oceanic upper layer. One important responding is the decreasing of SST due to the strong vertical mixing caused by typhoon (Price et al., 1994). According to the SST observation from the satellite, SST usually decreases 2-5℃ due to typhoon passing (Cione and Uhlhorn, 2003; D'Asaro et al., 2007; Wu et al., 2008; Jiang et al., 2009). Dare and Mcbride (2011) researched the response of SST to the global typhoons during 1981~2008 and indicated that the maximum decreasing of SST usually occurred in 1-day after typhoon passing.

In this section, we select the typhoon Tembin as an example to validate the MO and SCSOFS model skill for the SST simulation. As shown in Fig. 11, the typhoon Tembin went through and made a perfect turn around in the NSCS from 25 to 28 August 2012. From the three results, we can find the obvious decreasing of SST 1-day after typhoon passing, which is about 2-4℃ and well correspondence with previous studies mentioned in above. SCSOFS is much better agreement with OISST than MO, especially on 26 and 27 August 2012, not only for the range of SST decreasing, but also for the domain of SST deceasing.

3.3.3 Mesoscale eddy

Mesoscale eddies cannot be identified and extracted from geophysical turbulent flow as observed by satellite altimetry without suitable definition and a competitive identification algorithm. A multitude of

Nat. Hazards Earth Syst. Sci. Discuss., doi:10.5194/nhess-2016-60, 2016
Manuscript under review for journal Nat. Hazards Earth Syst. Sci.
Published: 25 February 2016
© Author(s) 2016. CC-BY 3.0 License.

different techniques for automatic identification of eddies have been proposed based either on physical or geometric criteria of the flow field. In this study, a free-threshold eddy identification algorithm with the SLA data is employed. This algorithm is based on the vector geometry method and Okubo-Weiss method (Okubo, 1970;) with six constraints applied to the SLA to detect an eddy: (1) a vorticity-dominated region at the eddy center ($W < 0$) must exist; (2) the SLA magnitude has a local extreme value (minimum or maximum); (3) closed contours of SLA around the eddy center must exist; (4) the eddy radius must be larger than 45km.(5)the eddy amplitude must be larger than 4cm. In this study, the amplitude is defined as the absolute value of the SLA difference between the eddy center and the SLA along the eddy edge. The Eddy-tracking method used is the one developed by Chaigneau et al. (2008), and we only keep eddies with life span not less than 28 days. Eddies were analyzed and compared based on MO, AVISO and SCSOFS in 2012. The numbers of eddies for three types of data were in Table 1, cyclones and anti-cyclones were counted separately and seasonally.

The spatial distribution of eddy birthplace is shown in Fig 12. MO has more eddies formed, especially anti-cyclones formed than those of AVISO, most of the excessive eddy cores were found near the middle of SCS. SCSOFS has more anti-cyclones as well and less cyclones than AVISO. Both MO and SCSOFS show excessive eddies formed in the middle of the basin and less eddies in the western of the east of Vietnam. The SLA of SCSOFS and MO is calculated simply by subtracting mean SSH (24 years mean for SCSOFS and only one-year mean for MO) instead of an uniformed Mean Sea Surface, which might cause the excessive anti-cyclones in both models. All three types of data agree that less eddies formed in the middle part of NSCS.

As for the seasonal distributions (figures not shown), all three data have most eddies in spring and lest in fall. Both AVISO and SCSOFS have more cyclones than anti-cyclones in spring and fall, and all three have less cyclones in summer. SCSOFS differs with AVISO mainly in winter while they agree reasonably in the other three seasons. MO has surplus eddies counted in every season especially for anti-cyclones, which might because of the error introduced by the simplified calculation of SLA.

4 Conclusions

Two operational ocean analysis and forecasting systems, MO and SCSOFS, have been built based on the state-of-the-art hydrodynamic ocean model in France and China, respectively. The comparison and

Nat. Hazards Earth Syst. Sci. Discuss., doi:10.5194/nhess-2016-60, 2016
Manuscript under review for journal Nat. Hazards Earth Syst. Sci.
Published: 25 February 2016
© Author(s) 2016. CC-BY 3.0 License.

validation for the performance of both systems on the ocean circulation, the structures of the TS, and mesoscale activities in the SCS, based on the observed satellite and *in-situ* data in 2012, are shown in this paper. The comprehensive performances for the both systems are summarized as follow.

Both systems have caught the main basin-scale circulations in the SCS and been well agreement with the result of AVISO. And the results of MO are better agreement with those of AVISO than those of SCSOFS for several branches and eddies in January. There are no many mesoscale or small scale circulations shown in SCSOFS, which may because of a little strong horizontal mixing set in the model. The westward intensification in the eastern coast of the Vietnam is most strong in autumn among the four seasons. For the type of the Kuroshio intruding the SCS, the three results show the looping path in winter, the leaping path in summer and leaking path in autumn. However, the leaking path, looping path and leaping path are shown for AVISO, MO and SCSOFS in spring, respectively.

Both systems get the same variation of the u-/v- components time series with the mooring observation. The RMSE between MO, SCSOFS and mooring observation are 0.075m/s, 0.094m/s for u-component, 0.062m/s, 0.084m/s for v-component, respectively. The results of MO are better agreement with the observation than those of SCSOFS, especially during the period of the Typhoon Kai-tak.

The maximum, minimum, and mean monthly RMSE between MO and MGDSST are 0.78℃, 0.37℃, 0.51℃, between SCSOFS and MGDSST are 1.15℃, 0.56℃, 0.86℃ for the SCSOFS in the SCS, respectively. For the horizontal and vertical distributions of TS, both systems have got the same structures with the *in-situ*, but the results of SCSOFS are better agreement with the *in-situ* than those of MO. The correlation coefficients of temperature are 0.987, 0.982, and of salinity are 0.717, 0.897, between MO, SCSOFS and *in-situ*, over the 95% significance level, respectively. It indicates that the good relativity between MO, SCSOFS and *in-situ*, the relativity of temperature is better agreement with *in-situ* than those of salinity for both MO and SCSOFS, and SCSOFS is better agreement with *in-situ* than MO for salinity.

The similar SST frontal patterns with their evident seasonal variations are shown in both systems. Most fronts achieve maximum strength in winter, become weak obviously due to the weakening of northeast monsoon EAM in spring and summer, fade and disappear in autumn. It is well agreement with the result of Wang et al. (2001).

During the typhoon Tembin in the NSCS, the obvious decreasing of SST about 2-4℃ occurs 1-day after typhoon passing shown in the results of MO, SCSOFS and OISST, which is well agreement with

Nat. Hazards Earth Syst. Sci. Discuss., doi:10.5194/nhess-2016-60, 2016
Manuscript under review for journal Nat. Hazards Earth Syst. Sci.
Published: 25 February 2016
© Author(s) 2016. CC-BY 3.0 License.

previous studies. SCSOFS is much better agreement with OISST than MO both for the range and domain of SST decreasing.

MO has more eddies formed near the middle of SCS than AVISO, especially for anti-cyclones. SCSOFS has more anti-cyclones as well, but less cyclones than AVISO. All three data have most eddies in spring and lest in fall, and less cyclones than anti-cyclones in summer. Both AVISO and SCSOFS have more cyclones than anti-cyclones in spring and fall.

In order to improve their performances further in the SCS, according to the comparison and validation for the two systems, MO and SCSOFS, we would like to propose some suggestions to modify the systems. For MO, we would like to suggest (1) to modify the model bathymetry in the coast area for the depth less than 200m to improve the model performance in shallow water area, such as SST front; (2) to change the initial conditions of TS to improve the TS vertical structures, especially for the salinity in deep water area; For SCSOFS, we would like to suggest (1) to weaken horizontal mixing to get more reasonable mesoscale or small scale circulations; (2) to optimize the data assimilation scheme further to better assimilate the *in-situ* and satellite data; (3) to replace the surface forcing data with the higher horizontal or temporal resolution; (4) to replace the boundary conditions from monthly to weekly or daily, such as MO. For both systems, we also would like to suggest to try to get and assimilate more observed data during the typhoon period to catch the typhoon process more exactly.

Author contribution

X. Zhu, H. Wang and G. Liu compared and validated the model results on velocities and TS. C. Régnier and M. Drévillon build the MO, D. Wang build the SCSOFS. X. Kuang analyzed the model results on mesoscale eddy. S. Ren analyzed the model results on SST front. Z. Jing provided the *in-situ* data. X. Zhu prepared the manuscript with contributions from all co-authors.

Acknowledgements

We would like to thank the anonymous reviewers and the Editor, , for their valuable contributions that allow us to improve the manuscript substantially. This study is supported by the National Natural Science Foundation of China under contract No. 41222038, 41376016, 41206023 and the Strategic Priority Research Program of the Chinese Academy of Sciences Grant No. XDA1102010403.

Nat. Hazards Earth Syst. Sci. Discuss., doi:10.5194/nhess-2016-60, 2016
Manuscript under review for journal Nat. Hazards Earth Syst. Sci.
Published: 25 February 2016
© Author(s) 2016. CC-BY 3.0 License.

Natural Hazards and Earth System Sciences Discussions

456 **References**

457 Arakawa, A. and Lamb, V. R.: Computational design of the basic dynamical processes of the UCLA
458 general circulation model. Methods of Computational Physics, 17. New York: Academic Press, 173–
459 265,1977.
460 Amante, C. and Eakins, B.: ETOPO1 1 Arc-Minute Global Relief Model: Procedures, Data Sources and
461 Analysis. NOAA Technical Memorandum NESDIS NGDC–24. National Geophysical Data Center,
462 NOAA, doi:10.7289/V5C8276M, 2009.
463 Barnier, B., Madec, G., Penduff, T., Molines, J. M., Treguier, A. M., Le Sommer, J., Beckmann, A.,
464 Biastoch, A., Boning, C., Deng, J., Derval, C., Durand, E., Gulev, S., Remy, E., Talandier, C., Theetten,
465 S., Maltrud, M., McClean, J., and De Cuevas, B.: Impact of partial steps and momentum advection
466 schemes in a global circulation model at eddy permitting resolution, Ocean Dynam., 56, 543–567, 2006.
467 Belkin, I. and Cornillon, P.: SST fronts of the pacific coastal and marginal seas. Pacific Oceanogr.,
468 1(2):90–113, 2003.
469 Bell, M. J., Schiller, A., Traon, P. Y. Le, Smith, N. R., Dombrowsky, E. and WilmerBecker, K.: An
470 introduction to GODAE OceanView. Journal of Operational Oceanography, 8, sup1, s2–s11, doi:
471 10.1080/1755876X.2015.1022041, 2015.
472 Blanke, B. and Delecluse, P.: Variability of the tropical Atlantic-Ocean simulated by a general-
473 circulation model with 2 different mixed-layer physics, J. Phys. Oceanogr., 23, 1363–1388, 1993.
474 Cai, S. and Wang, W.: A numerical study on the circulation mechanism in the northeastern South China
475 Sea and Taiwan Strait. Tropic Oceanology, 16(1), 7–15, 1997. (in Chinese with English abstract).
476 Carton, J. and Giese, B.: A Reanalysis of Ocean Climate Using Simple Ocean Data Assimilation
477 (SODA). Mon. Weath. Rev., 136, 2999–3017, doi: 10.1175/2007MWR1978.1, 2008.
478 Caruso, M., Gawarkiewicz, G. and Beardsley, R.: Interannual variability of the Kuroshio intrusion in the
479 South China Sea. J Oceanogr., 62(4), 559–575, 2006.
480 Chaigneau, A., Gizolme, A. and Grados, C.: Mesoscale eddies off Peru in altimeter records:
481 Identification algorithms and eddy spatiotemporal patterns, Prog. Oceanogr., 79, 106–119, 2008.
482 Chao, S.，Shaw, P. and Wang, J.: Wind relaxation as a possible cause of the South China Sea Warm
483 Current. J. Oceanogr., 51(1), 111–132, 1995.

© Author(s) 2016. CC-BY 3.0 License.

484 Chao, S., Shaw, P. and Wu, S.: Deep water ventilation in the South China Sea. Deep Sea Res. I, 43, 445–
485 466, 1996.
486 Chern, C. and Wang, J.: A numerical study of the summertime flow around the Luzon Strait. J. Oceanogr.,
487 54(1), 53–64, 1998.
488 Chern, C. and Wang, J.: Numerical study of the upper-layer circulation in the South China Sea. J
489 Oceanogr., 59, 11–24, 2003.
490 Chern, C., Jan, S. and Wang, J.: Numerical study of mean flow patterns in the South China Sea and the
491 Luzon Strait, Ocean Dynamics, 60, 1 047–1 059, doi:10.1007/s10236-010-0305-3, 2010.
492 Chu, P. and Fan, C.: A low salinity cool-core cyclonic eddy detected northwest of Luzon during the
493 South China Sea Monsoon Experiment (SCSMEX) in July 1998, J. Oceanogr., 57, 549–563,
494 doi:10.1023/A:1021251519067, 2001.
495 Chu, P. and Li, R.: South China Sea Isopycnal-Surface Circulation. J. Phys. Oceanogr., 30, 2420–2438,
496 2000.
497 Chu, P., Lu, S. and Chen, Y.: A Coastal Air-Ocean Coupled System (CAOCS) evaluated using an
498 Airborne Expendable Bathythermograph (AXBT) data set, J. Oceanogr., 55, 543–558,
499 doi:10.1023/A:1007847609139, 1999.
500 Cione, J. and Uhlhorn, E.: Sea surface temperature variability in hurricanes: Implications with respect to
501 intensity change. Monthly Weather Review, 131(8), 1783–1796, 2003.
502 CLS, SSALTO/DUACS User handbook: (M)SLA and (M)ADT Near-Real Time and Delayed Time
503 Products. CLS-DOS-NT-06-034, Issue 4.4, Nomenclature: SALP-MU-P-EA-21065-CLS, 2015.
504 Dare, R. and Mcbride, J.: Sea surface temperature response to tropical cyclones. Monthly Weather
505 Review, 139(12), 3798–3808, 2011.
506 D'Asaro, E., Sanford, T., Niiler, P., Terrill, E.: Cold wake of hurricane Frances. Geophys. Res. Lett.,
507 34(15), L15609, 2007.
508 Du, Y., Yi, J., Wu, D., He, Z., Wang, D., Liang, F.: Mesoscale oceanic eddies in the South China Sea
509 from 1992 to 2012: evolution processes and statistical analysis. Acta Oceanologica Sinica, 33(11), 36–
510 47, doi: 10.1007/s13131-014-0530-6, 2014.
511 Fang, G. and Zhao, B.: A note on the main forcing of the northeastward flowing current off the Southeast
512 China Coast. Prog. Oceanog., 21, 363–372, 1988.

© Author(s) 2016. CC-BY 3.0 License.

513 Fang, Y., Fang, G. and Yu, K.: ADI barotropic ocean model for simulation of Kuroshio intrusion into
514 China southeastern waters. Chin. J. Oceanol. Limnol., 14(4), 357–366, 1996.
515 Farris, A. and Wimbush, M.: Wind-induced intrusion into the South China Sea. J. Oceanogr., 52, 771–
516 784, 1996.
517 Fichefet, T. and Maqueda, M. A.: Sensitivity of a global sea ice model to the treatment of ice
518 thermodynamics and dynamics, J. Geophys. Res., 102, 12609–12646, 1997.
519 Goosse, H., Campin, J. M., Deleersnijder, E., Fichefet, T., Mathieu, P. P., Maqueda, M. A. M., and
520 Tartinville, B.: Description of the CLIO model version 3.0, Institut d'Astronomie et de Geophysique
521 Georges Lemaitre, Catholic University of Louvain (Belgium), 2001.
522 Guan, B.: The warm current in the South China Sea——a current flowing against the wind in winter in
523 the open sea off Guangdong province. Oceanologia et Limnologia Sinica, 9(2), 117–127, 1978 (in
524 Chinese with English abstract).
525 Guan, B.: Winter counter—wind current off the south eastern China coast and a preliminary
526 investigation of its source. Proceedings of the Symposium on the Physical and Chemical Oceanography
527 of the China Seas. Beijing, China Ocean Press, 1–9, 1993.
528 Hellerman, S. and Rosenstein, M.: Normal monthly wind stress over the world ocean with error estimates.
529 J. Phys. Oceanogr., 13, 1 093–1 104, 1983.
530 Hu, J., Liang, H. and Zhang, X.: Sectional distribution of salinity and its indication of Kuroshio's
531 intrusion in southern Taiwan Strait and northern South China Sea late summer, 1994. Acta Oceanologica
532 Sinica, 18(2), 225–236, 1999.
533 Hu, J., Kawamura, H., Hong, H. and Qi, Y.: A review on the currents in the South China Sea: seasonal
534 circulation, South China Sea Current and Kuroshio intrusion. J. Oceanogr., 56, 607–624, 2000.
535 Hu, J., Gan, J., Sun, Z., Zhu, J. and Dai, M.: Observed three dimensional structure of a cold eddy in the
536 southwestern South China Sea, J. Geophys. Res., 116, C05016, doi:10.1029/2010JC006810, 2011.
537 Huang, Q., Wang, W., Li, Y., Li, C. and Mao, M.: General situations of the current and eddy in the South
538 China Sea. Advance in Earth Sciences, 7(5), 1–9, 1992 (in Chinese with English abstract)
539 Hunke, E. C. and Dukowicz J. K.: An elastic-viscous-plastic model for sea ice dynamics, J. Phys.
540 Oceanogr., 27, 1849–1867, 1997.

© Author(s) 2016. CC-BY 3.0 License.

Ji, Q., Zhu, X., Wang, H., Liu, G., Gao, S., Ji, X. and Xu, Q.: Assimilating operational SST and sea ice analysis data into an operational circulation model for the coastal seas of China. Acta oceanologica Sinica, 34(7), 54–64, doi: 10.1007/s13131-015-0691-y, 2015.

Jiang, X., Zhong, Z. and Jiang, J.: Upper ocean response of the South China Sea to Typhoon Krovanh (2003). Dynamics of Atmospheres and Oceans, 47(1), 165–175, 2009.

Jing, Z. Y., Qi, Y. Q., Du, Y., Zhang, S. W. and Xie, L. L.: Summer upwelling and thermal fronts in the northwestern South China Sea: Observational analysis of two mesoscale mapping surveys. J. Geophys. Res. Oceans, 120, 1993-2006, doi:10.1002/2014JC010601, 2015.

Kanamitsu, M., Ebisuzaki, W., Woollen, J., Yang, S., Hnilo, J., Fiorino, M., and Potter, G.: NCEP-DOE AMIP-II Reanalysis (R-2). Bulletin of the American Meteorological Society, 1631–1643, Nov 2002.

Lellouche, J. M., Le Galloudec, O., Drévillon, M., Régnier, C., Greiner, E., Garric, G., Ferry, N., Desportes, C., Testut, C. E., Bricaud, C., Bourdalle-Badie, R., Tranchant, B., Benkiran, M., Drillet, Y., Daudin, A. and De Nicola, C.: Evaluation of global monitoring and forecasting systems at Mercator Ocean, Ocean Sci., 9, 57–81, doi:10.5194/os-9-57-2013, 2013

Li, R., Zeng, Q., Gan, Z. and Wang, W.: Numerical simulation of South China Sea Warm Current and currents in Taiwan Strait in winter. Progress in Natural Sciences, 3(1), 21–25, 1993. (in Chinese with English abstract).

Li, L., Nowlin Jr., W. D. and Su, J.: Anticyclonic rings from the Kuroshio in the South China Sea. Deep-Sea Res. I, 45, 1469–1482, 1998a.

Li, W., Liu, Q. and Yang, H.: Principal features of ocean circulation in the Luzon Strait. Journal of Ocean University of Qingdao, 28(3), 345–352, 1998b (in Chinese with English abstract).

Liang, W., Yang, Y., Tang, T., and Chuang, W.: Kuroshio in the Luzon Strait. J. Geophys. Res., 113, C08048, doi:10.1029/2007JC004609, 2008.

Liu, Q., Liu, C., Zheng, S., Xu, Q. and Li, W.: The deformation of Kuroshio in the Luzon Strait and its dynamics. Journal of Ocean University of Qingdao, 26(4), 413–420, 1996. (in Chinese with English abstract).

Madec, G. and Imbard, M.: A global ocean mesh to overcome the North Pole singularity, Clim. Dynam., 12, 381–388, 1996.

© Author(s) 2016. CC-BY 3.0 License.

569 Mao, Q., Shi, P. and Qi, Y.: Sea surface dynamic topography and geostrophic current over the South
570 China Sea from Geosat altimeter observation. Acta Oceanologica Sinica, 21(1), 11–16, 1999. (in Chinese
571 with English abstract).
572 Nan, F., Xue, H., Chai, F., Shi, L., Shi, M. and Guo, P.: Identification of different types of Kuroshio
573 intrusion into the South China Sea. Ocean Dynamics, doi: 10.1007/s10236-011-0426-3, 2011a.
574 Nan, F., He, Z., Zhou, H. and Wang, D.: Three long-lived anticyclonic eddies in the northern South
575 China Sea, J. Geophys. Res., 116, C05002, doi:10.1029/2010JC006790, 2011b.
576 Nan, F., Xue, H., Chai, F., Wang, D., Yu, F., Shi, M., Guo, P. and Xiu, P.: Weakening of the Kuroshio
577 intrusion into the South China Sea over the past two decades. Journal of Climate, 26, 8097–8110, doi:
578 10.1175/JCLI-D-12-00315.1, 2013.
579 Nan, F., Xue, H. and Yu, F.: Kuroshio intrusion into the South China Sea: A review. Progress in
580 Oceanography, 137(A), 314–333, doi: 10.1016/j.pocean.2014.05.012, 2015.
581 Okubo, A.: Horizontal dispersion of floatable particles in the vicinity of velocity singularity such as
582 convergences. Deep Sea Research, 17, 445–454, 1970.
583 Pham, D. T., Verron, J., and Roubaud, M. C.: A singular evolutive extended Kalman filter for data
584 assimilation in oceanography, J. Mar. Syst., 16, 323–340, 1998.
585 Price, J., Sanford, T., Forristall, G.: Forced stage response to a moving hurricane. J. Phys. Oceanogr.,
586 24(2), 233–260, 1994.
587 Qu, T.: Upper-layer circulation in the South China Sea. J. Phys. Oceanogr., 90, 1450–1460, 2000.
588 Qu, T., Mitsudera, H. and Yamagata, T.: Intrusion of the North Pacific waters into the South China Sea.
589 J. Geophys. Res., 105(C3), 6415–6424, 2000.
590 Rio, M. H., Hernandez F.: A mean dynamic topography computed over the world ocean from altimetry,
591 in situ measurements, and a geoid model, J. Geophys. Res., 109, C12032, 2004
592 Roullet, G. and Madec, G.: Salt conservation, free surface, and varying levels: a new formulation for
593 ocean general circulation models, J. Geophys. Res., 105, 23927–23942, 2000.
594 Shapiro, R.: Linear Filtering. Math. Comput., 29, 1094–1097, 1975.
595 Shchepetkin, A. and McWilliams, J.: The regional oceanic modeling system (ROMS): a split-explicit,
596 free-surface, topography-following-coordinate oceanic model. Ocean Modell., 9, 347–404,
597 doi:10.1016/j.ocemod.2004.08.002, 2005.

© Author(s) 2016. CC-BY 3.0 License.

598 Su, J.: Overview of the South China Sea circulation and its dynamics. Acta Oceanologica Sinica, 27(6),
599 1–8, 2005.
600 Takano, K., Harashima, A. and Namba, T.: A numerical simulation of the circulation in the South China
601 Sea—preliminary results. Acta Oceanogr. Taiwanica, 37, 165–186, 1998.
602 Wang, D., Liu, Y., Qi, Y., and Shi, P.: Seasonal variability of thermal fronts in the northern South China
603 Sea from satellite data. Geophys. Res. Lett., 28(20), 3963–3966, 2001.
604 Wang, D., Xu, H., Lin, J. and Hu, J.: Anticyclonic eddies in the northeastern South China Sea during
605 winter 2003/2004. J. of Oceanogr., 64(6), 925–935, 2008.
606 Wang, G., Su, J. and Chu P.: Mesoscale eddies in the South China Sea observed with altimeter data,
607 Geophys. Res. Lett., 30(21), 2121, doi:10.1029/2003GL018532, 2003.
608 Wang, G., Chen, D. and Su, J.: Winter eddy genesis in the Eastern South China Sea due to orographic
609 wind jets. J. of Phys. Oceanogr., 38(3), 726–732, 2008
610 Wang, J.: Global linear stability of the 2-D shallow-water equations: An application of the distributive
611 theorem of roots for polynomials in the unit circle. Mon. Wea. Rev., 124, 1301–1310, 1996.
612 Wang, J. and Chern, C.: The warm-core eddy in the northern South China Sea, I. Preliminary
613 observations on the warm-core eddy, Acta Oceanogr. Taiwan, 18, 92–103, 1987. (in Chinese with
614 English abstract)
615 Weiss, J.: The dynamics of enstrophy transfer in two dimensional hydrodynamics. Physica D., 48, 273–
616 294, 1991.
617 Williamson, G.: Hydrography and weather of the Hong Kong fishing ground. Hong Kong Fisheries
618 Bulletin, 1, 43–49, 1970.
619 Wu, C. and Chiang, T.: Mesoscale eddies in the northern South China Sea. Deep-Sea Res. II, 54, 1575–
620 1588, 2007.
621 Wu, C., Shaw, P. and Chao, S.: Assimilating altimetric data into a South China Sea model. J. Geophys.
622 Res., 104(C12), 29987–30005, 1999.
623 Wu, C., Chang, Y., Oey, L., et al.: Air-sea interaction between tropical cyclone Nari and Kuroshio.
624 Geophys. Res. Lett., 35(12), L12605, 2008.
625 Wyrtki, K.: Scientific results of marine investigation of the South China Sea and Gulf of Thailand. Naga
626 Rep. 2, 195, 1961.

Nat. Hazards Earth Syst. Sci. Discuss., doi:10.5194/nhess-2016-60, 2016
Manuscript under review for journal Nat. Hazards Earth Syst. Sci.
Published: 25 February 2016
© Author(s) 2016. CC-BY 3.0 License.

627 Xiu, P., Chai, F., Shi, L., Xue, H. and Chao, Y.: A census of eddy activities in the South China Sea during
628 1993–2007. J. Geophys. Res., 115, C03012, doi:10.1029/2009JC005657, 2010.
629 Zhang, F., Wang, W., Huang, Q., Li, Y. and Chau, K.: Summary current structure in Bashi Channel. In
630 Proceedings of Symposium of Marine Sciences in Taiwan Strait and Its Adjacent Waters, 65–72, China
631 Ocean Press, Beijing, 1995.
632 Zhang, Z., Zhao, W., Tian, J. and Liang, X.: A mesoscale eddy pair southwest of Taiwan and its influence
633 on deep circulation, J. Geophys. Res. Oceans, 118, 6479–6494, doi:10.1002/2013JC008994, 2013.
634 Zhuang, W., Xie, S., Wang, D., Taguchi, B., Aiki, H. and Sasaki H.: Intraseasonal variability in sea
635 surface height over the South China Sea, J. Geophys. Res., 115, C04010, doi:10.1029/2009JC005647,
636 2010.
637
638
639
640
641
642
643
644
645
646
647
648
649
650
651
652
653
654
655
656
657
658
659
660
661
662
663
664
665

Nat. Hazards Earth Syst. Sci. Discuss., doi:10.5194/nhess-2016-60, 2016
Manuscript under review for journal Nat. Hazards Earth Syst. Sci.
Published: 25 February 2016
© Author(s) 2016. CC-BY 3.0 License.

Natural Hazards and Earth System Sciences
Discussions

666
667
668
669
670

Table 1 Eddy Numbers of different datatype

	AVISO			MO			SCSOFS		
	CYCL	ACYCL	TOTAL	CYCL	ACYCL	TOTAL	CYCL	ACYCL	TOTAL
Spring	6	3	9	6	7	13	6	3	9
Summer	2	3	5	4	7	11	3	5	8
Fall	2	1	3	6	7	13	2	1	3
Winter	5	2	7	5	5	10	1	3	4
Overall	15	9	24	21	26	47	12	12	24

671

Nat. Hazards Earth Syst. Sci. Discuss., doi:10.5194/nhess-2016-60, 2016
Manuscript under review for journal Nat. Hazards Earth Syst. Sci.
Published: 25 February 2016
© Author(s) 2016. CC-BY 3.0 License.

Natural Hazards and Earth System Sciences
Discussions

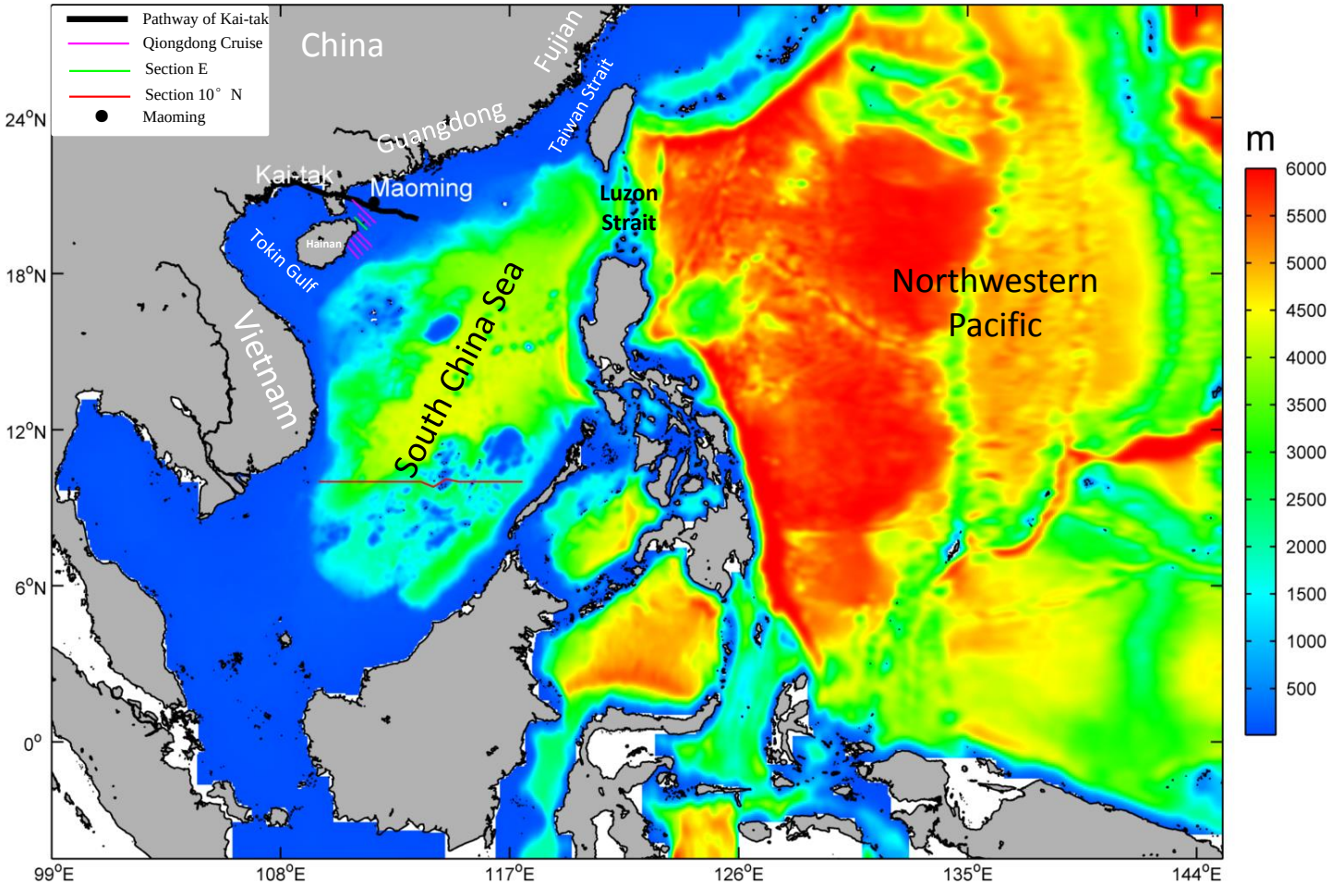

Figure 1: The model domain and bathymetry of SCSOFS.

Nat. Hazards Earth Syst. Sci. Discuss., doi:10.5194/nhess-2016-60, 2016
Manuscript under review for journal Nat. Hazards Earth Syst. Sci.
Published: 25 February 2016
© Author(s) 2016. CC-BY 3.0 License.

Natural Hazards and Earth System Sciences
Discussions

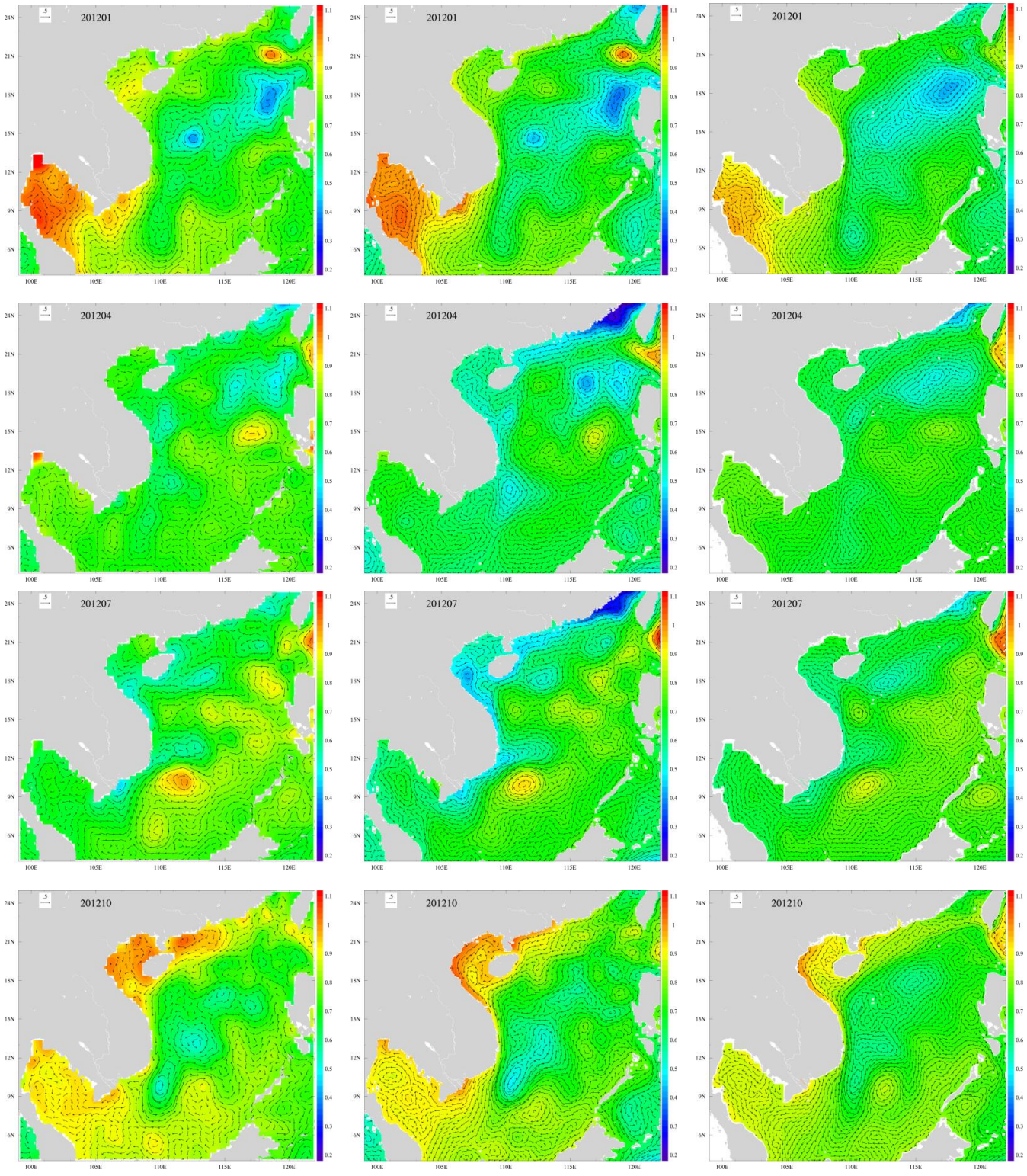

Figure 2: The monthly mean Sea Surface Height (color shaded) and the corresponding surface absolute geostrophic velocity (units: m s^{-1}) in January, April, July, and October, 2012. The left panels are from AVISO, the middle panels are from Mercator Océan, the right panels are from SCSOFS.

Nat. Hazards Earth Syst. Sci. Discuss., doi:10.5194/nhess-2016-60, 2016
Manuscript under review for journal Nat. Hazards Earth Syst. Sci.
Published: 25 February 2016
© Author(s) 2016. CC-BY 3.0 License.

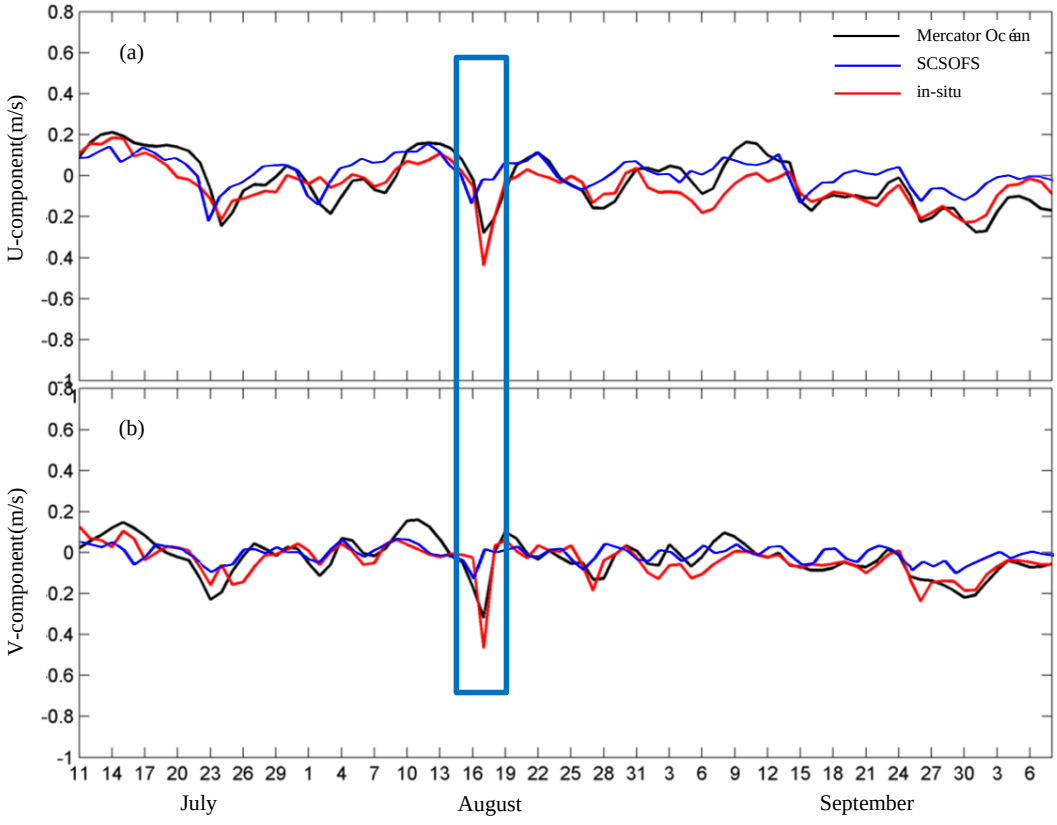

Figure 3: The daily mean time series of u(a) and v(b) components in 40m-depth layer at the Maoming mooring station, from in-situ, Mercator Océan, and SCSOFS.

Nat. Hazards Earth Syst. Sci. Discuss., doi:10.5194/nhess-2016-60, 2016
Manuscript under review for journal Nat. Hazards Earth Syst. Sci.
Published: 25 February 2016
© Author(s) 2016. CC-BY 3.0 License.

Natural Hazards and Earth System Sciences
Discussions

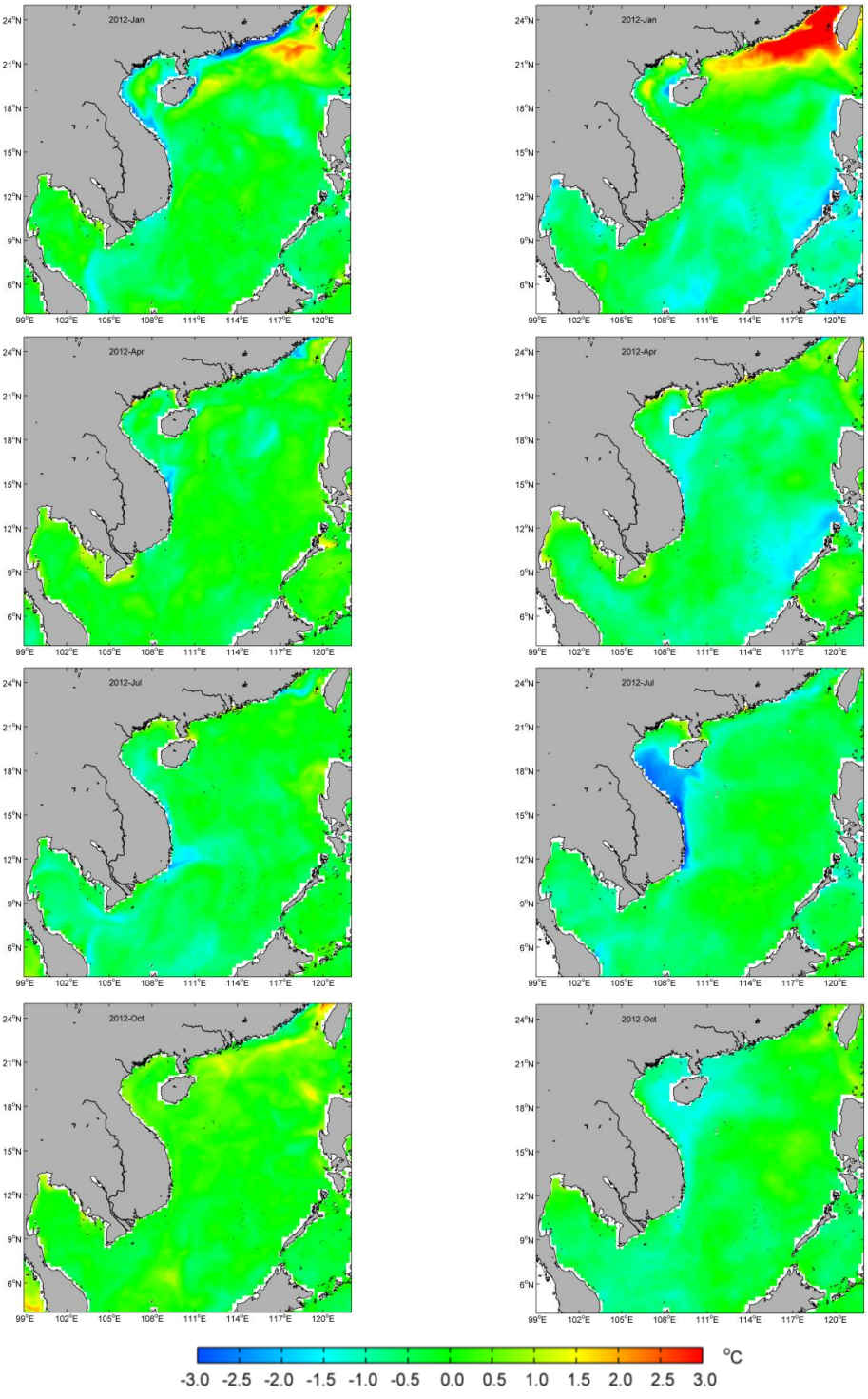

Figure 4: The monthly mean SST error between Mercator Océan (left panels), SCSOFS (right panels) and MGDSST in January, April, July, and October, 2012

Nat. Hazards Earth Syst. Sci. Discuss., doi:10.5194/nhess-2016-60, 2016
Manuscript under review for journal Nat. Hazards Earth Syst. Sci.
Published: 25 February 2016
© Author(s) 2016. CC-BY 3.0 License.

Natural Hazards and Earth System Sciences
Discussions

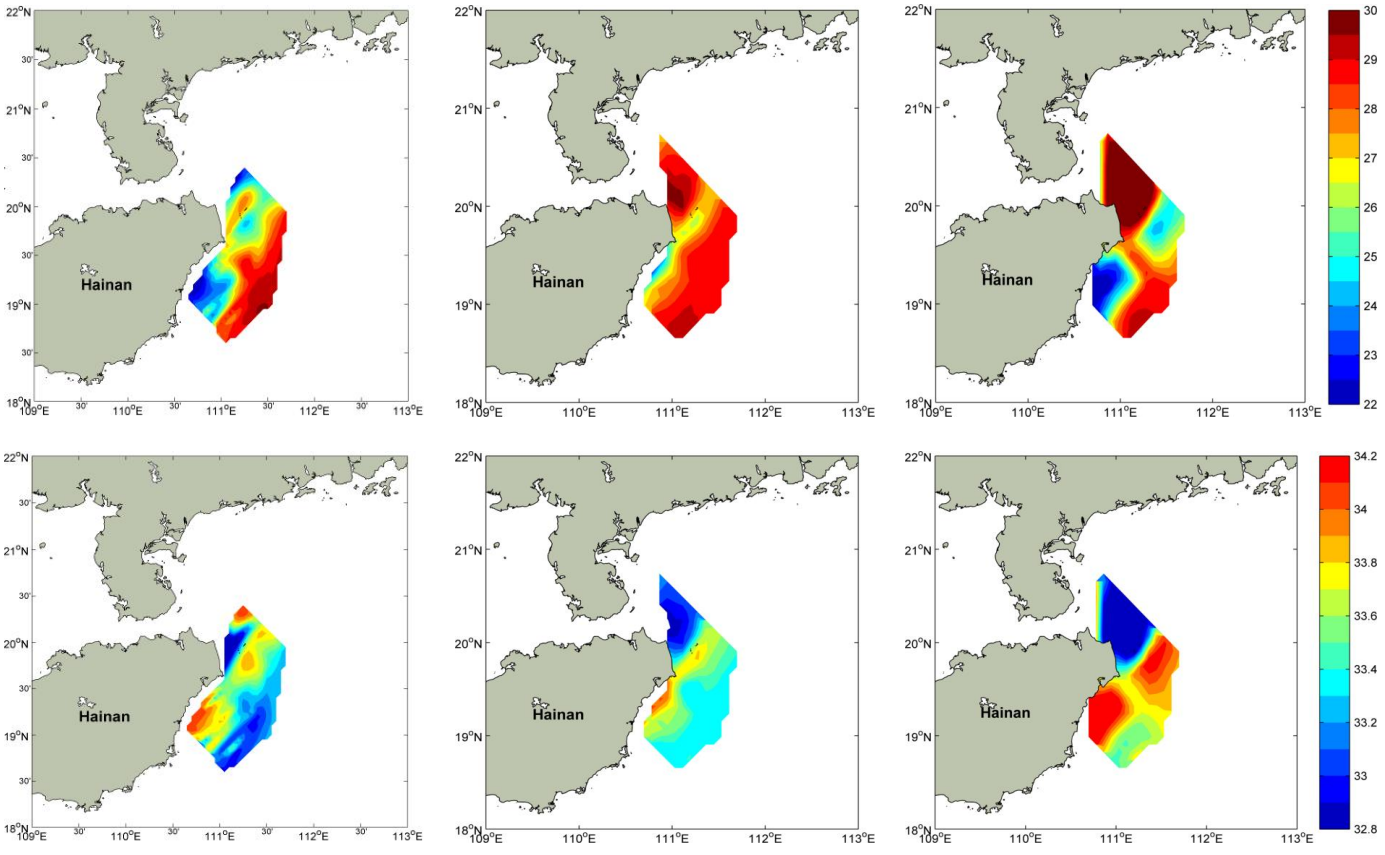

Figure 5: The horizontal distributions of temperature (upper panels) and salinity (lower panels) at 10-m depth layer from the *in-situ* observations of Qiongdong cruise (left column), Mercator Océan (middle column), and SCSOFS (right column), respectively.

Nat. Hazards Earth Syst. Sci. Discuss., doi:10.5194/nhess-2016-60, 2016
Manuscript under review for journal Nat. Hazards Earth Syst. Sci.
Published: 25 February 2016
© Author(s) 2016. CC-BY 3.0 License.

Natural Hazards and Earth System Sciences
Discussions

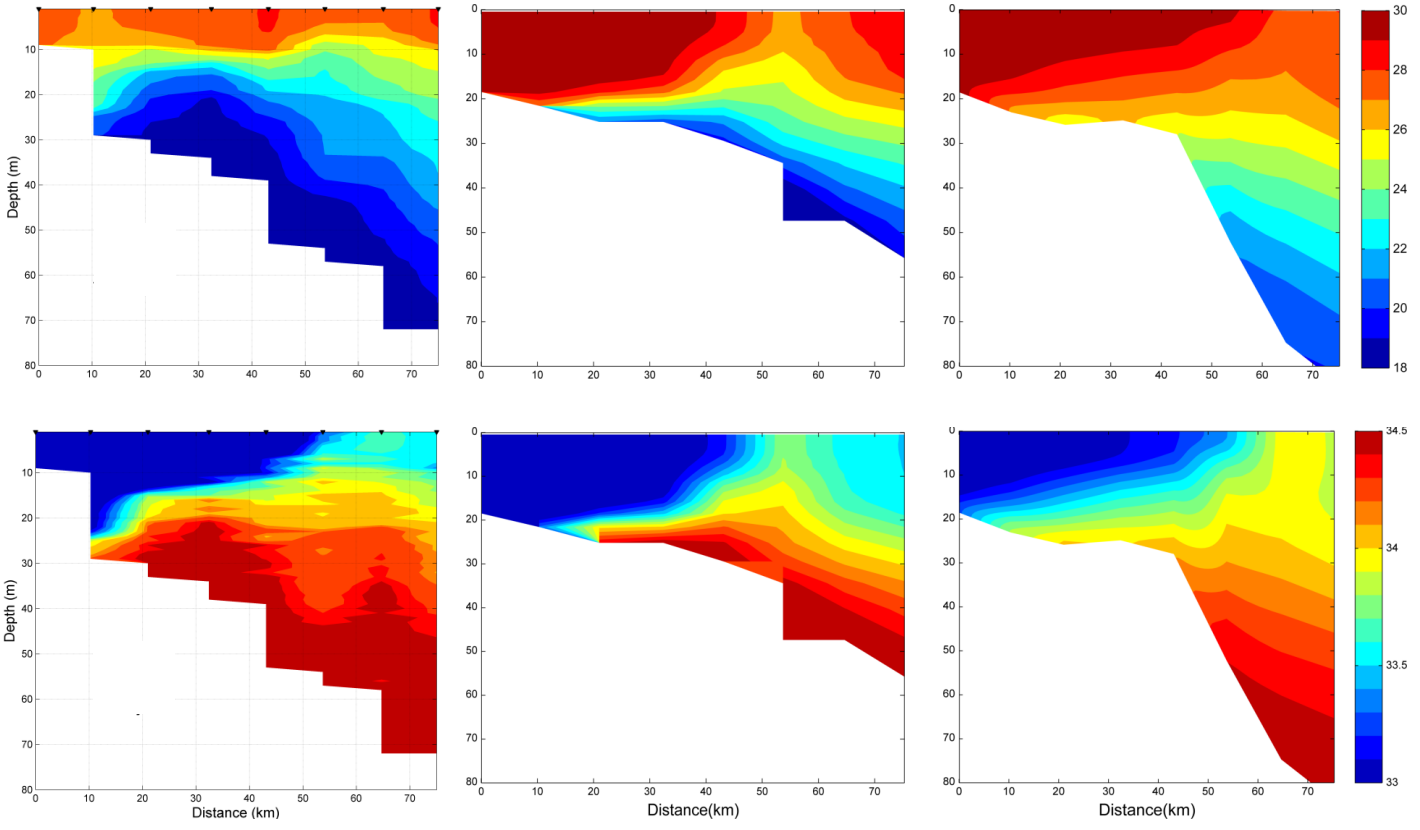

Figure 6: The vertical distributions of temperature (upper panels) and salinity (lower panels) along the section E (See Fig.1) from the *in-situ* observations of Qiongdong cruise (left column), Mercator Océan (middle column), and SCSOFS (right column), respectively.

Nat. Hazards Earth Syst. Sci. Discuss., doi:10.5194/nhess-2016-60, 2016
Manuscript under review for journal Nat. Hazards Earth Syst. Sci.
Published: 25 February 2016
© Author(s) 2016. CC-BY 3.0 License.

Natural Hazards and Earth System Sciences
Discussions

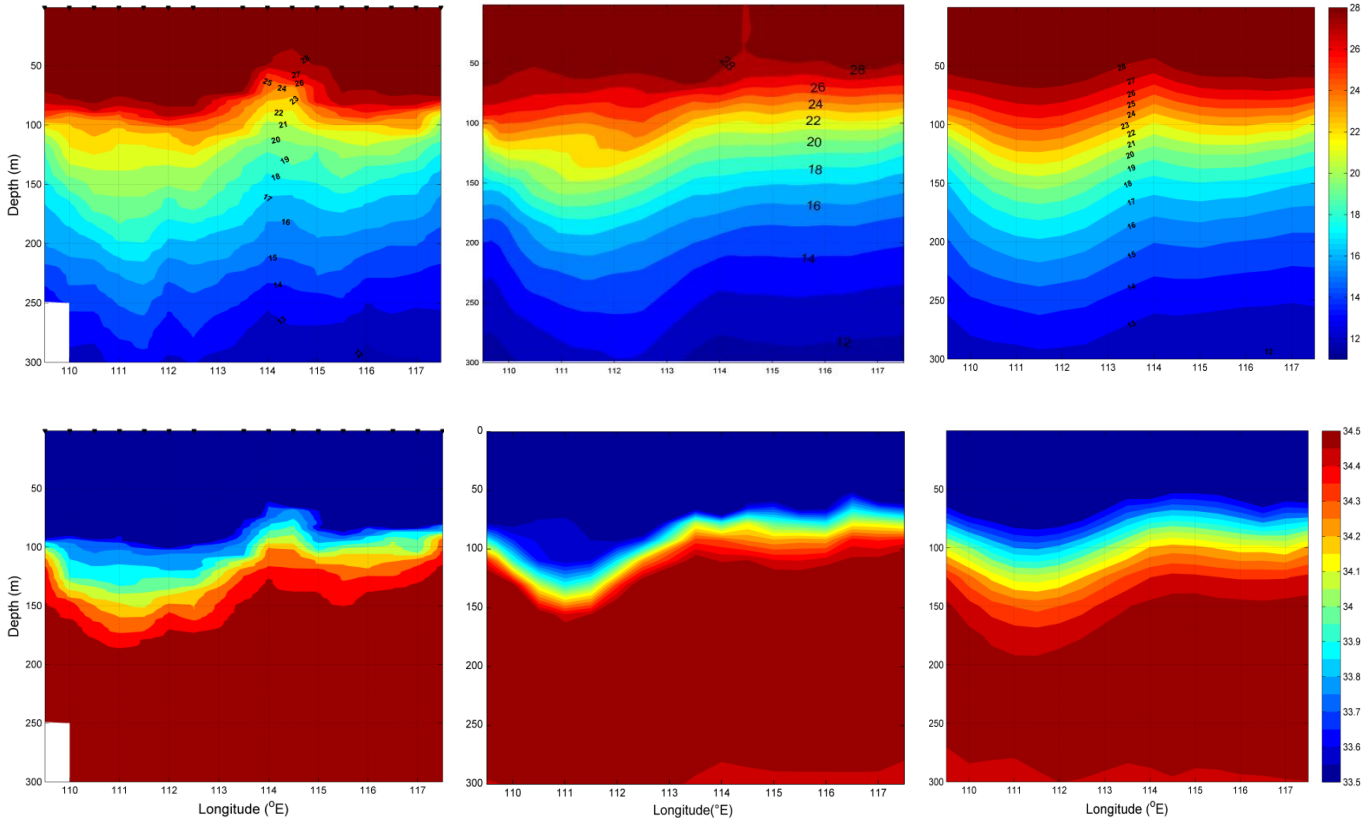

Figure 7: The vertical distributions of temperature (upper panels) and salinity (lower panels) in above 300m depth along the section 10° N from the *in-situ* observations of Nansha cruise (left column), Mercator Océan (middle column), and SCSOFS (right column), respectively.

Nat. Hazards Earth Syst. Sci. Discuss., doi:10.5194/nhess-2016-60, 2016
Manuscript under review for journal Nat. Hazards Earth Syst. Sci.
Published: 25 February 2016
© Author(s) 2016. CC-BY 3.0 License.

Natural Hazards and Earth System Sciences
Discussions

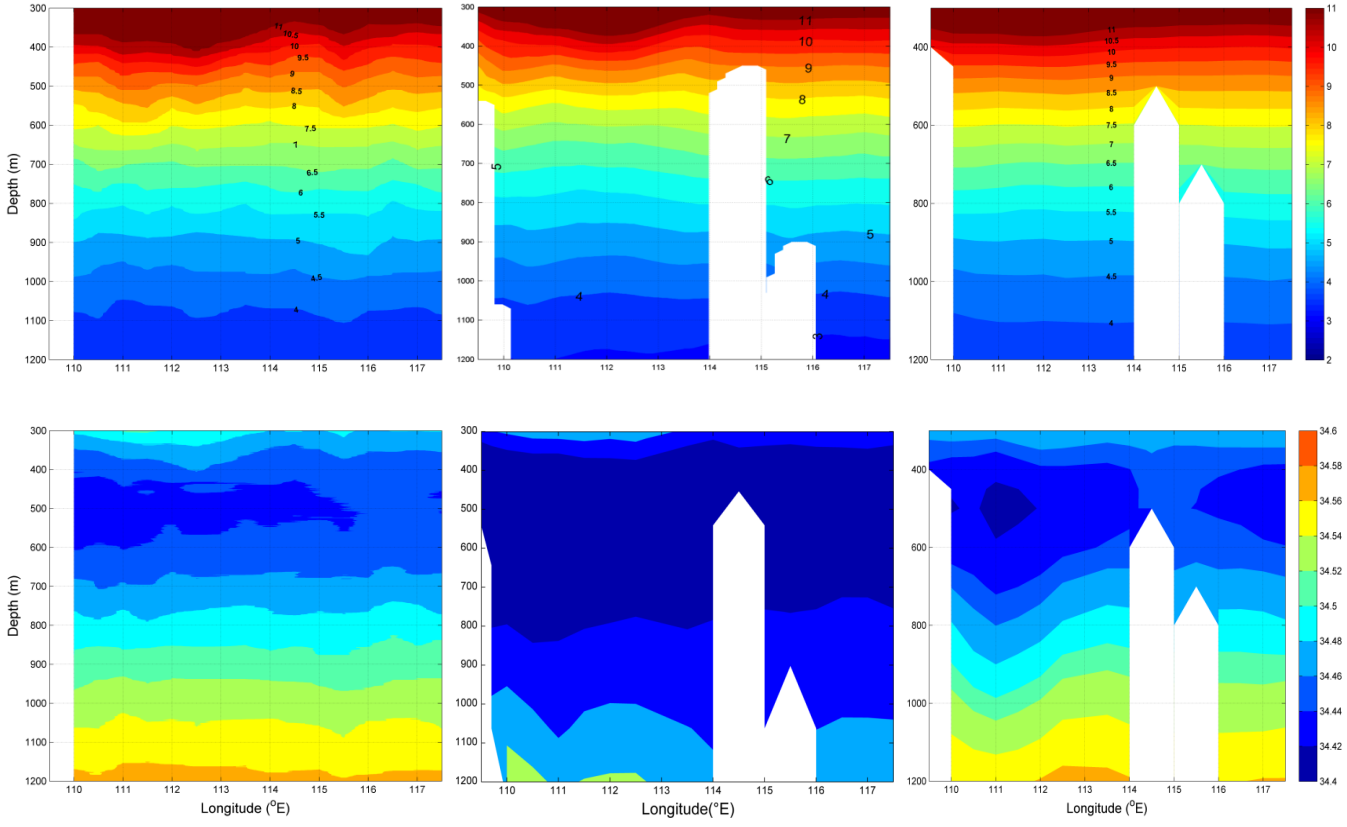

Figure 8: The same with Fig.7, but for the deep layer with depth from 300m to 1200m.

Nat. Hazards Earth Syst. Sci. Discuss., doi:10.5194/nhess-2016-60, 2016
Manuscript under review for journal Nat. Hazards Earth Syst. Sci.
Published: 25 February 2016
© Author(s) 2016. CC-BY 3.0 License.

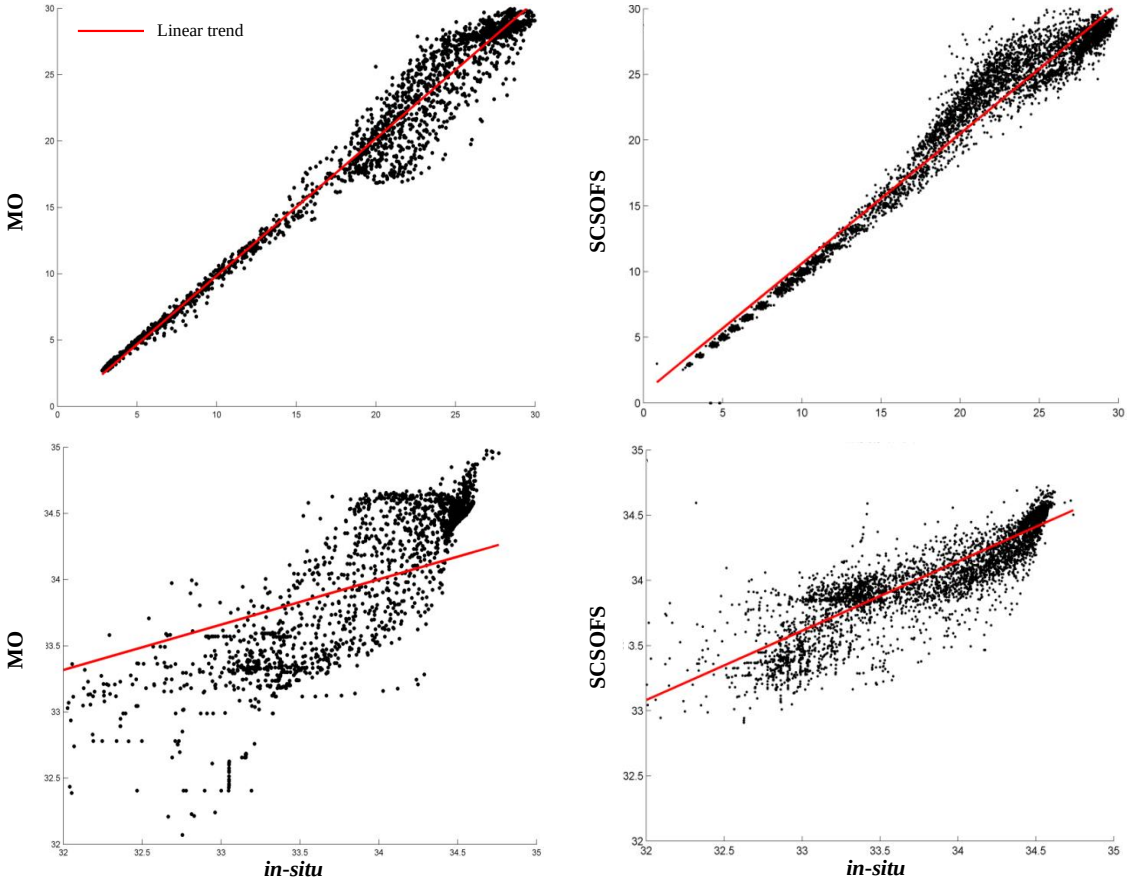

Figure 9: The relative relationships of temperature (upper panels) and salinity (lower panels) between Mercator Océan (left column), SCSOFS (right column) and the *in-situ* observations of all cruises.

Nat. Hazards Earth Syst. Sci. Discuss., doi:10.5194/nhess-2016-60, 2016
Manuscript under review for journal Nat. Hazards Earth Syst. Sci.
Published: 25 February 2016
© Author(s) 2016. CC-BY 3.0 License.

Natural Hazards and Earth System Sciences
Discussions

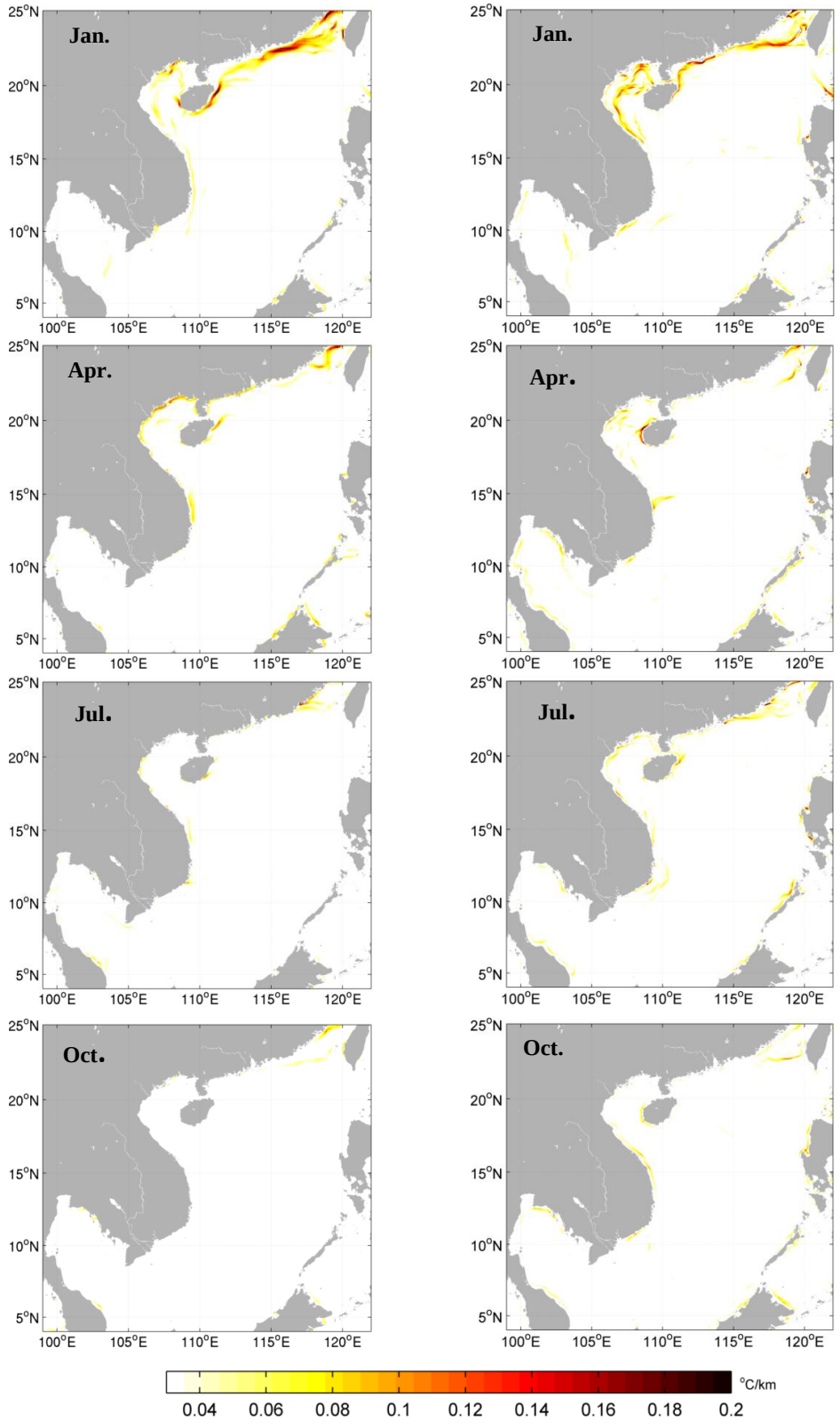

Figure 10: The distributions of SST fronts in the SCS from Mercator Océan (left panels) and SCSOFS (right panels) in January, April, July, and October.

Nat. Hazards Earth Syst. Sci. Discuss., doi:10.5194/nhess-2016-60, 2016
Manuscript under review for journal Nat. Hazards Earth Syst. Sci.
Published: 25 February 2016
© Author(s) 2016. CC-BY 3.0 License.

Natural Hazards and Earth System Sciences
Discussions

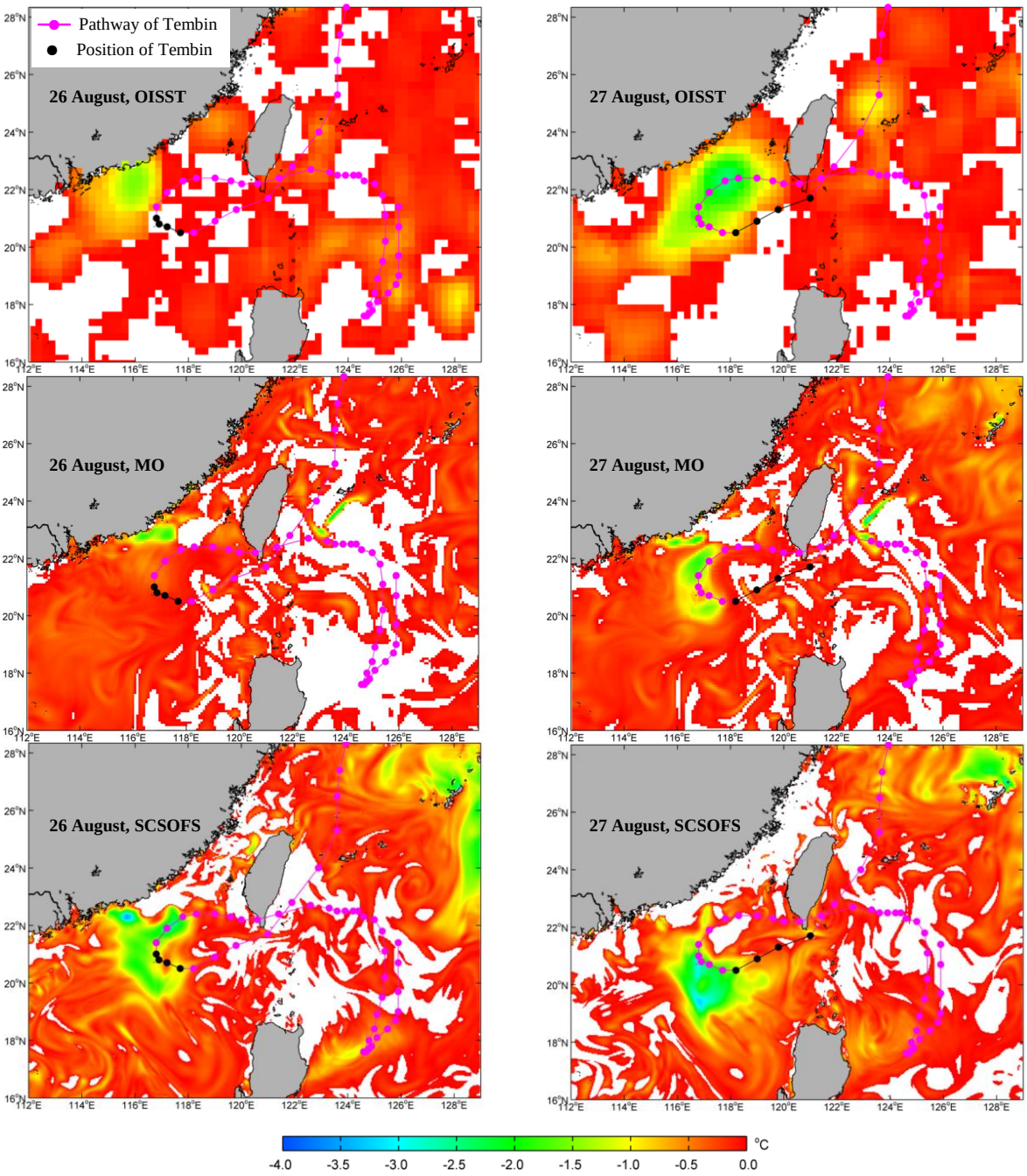

Figure 11: The SST differences of the day from the last day during the period of Typhoon Tembin. The black dots are the positions of the Typhoon Tembin at 00h, 06h, 12h, and 18h on each day.

Nat. Hazards Earth Syst. Sci. Discuss., doi:10.5194/nhess-2016-60, 2016
Manuscript under review for journal Nat. Hazards Earth Syst. Sci.
Published: 25 February 2016
© Author(s) 2016. CC-BY 3.0 License.

Natural Hazards and Earth System Sciences
Discussions

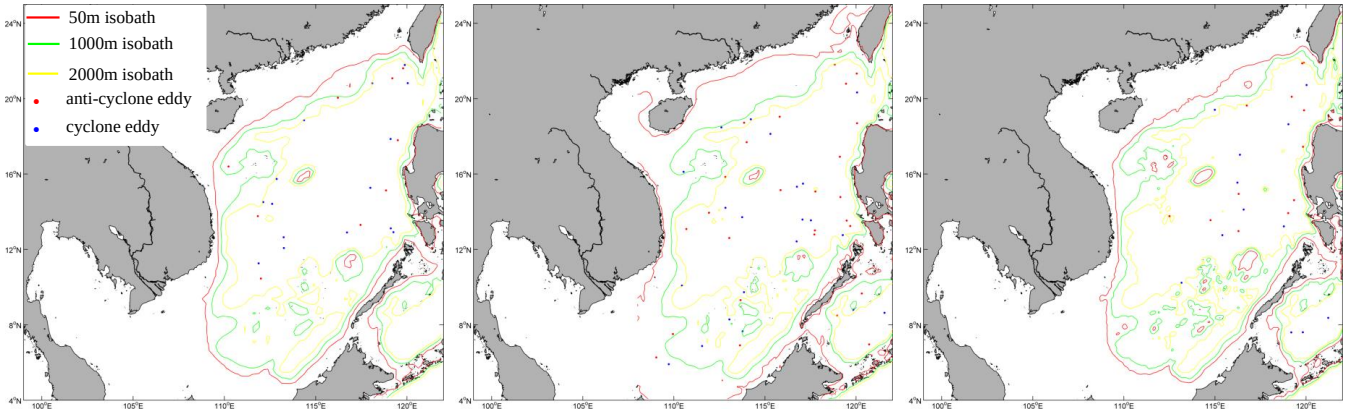

Figure 12: The spatial distributions of eddy birthplace identified using the method of Chaigneau et al. (2008) in the SCS from AVISO (left), Mercator Océan (middle) and SCSOFS (right) in 2012.